# Syndapin promotes pseudocleavage furrow formation by actin organization in the syncytial *Drosophila* embryo

Aparna Sherlekar and Richa Rikhy*
Biology, Indian Institute of Science Education and Research, Pashan, Pune 411008, India

**ABSTRACT** **Coordinated membrane and cytoskeletal remodeling activities are required for membrane extension in processes such as cytokinesis and syncytial nuclear division cycles in *Drosophila*. Pseudocleavage furrow membranes in the syncytial *Drosophila* blastoderm embryo show rapid extension and retraction regulated by actin-remodeling proteins. The F-BAR domain protein Syndapin (Synd) is involved in membrane tubulation, endocytosis, and, uniquely, in F-actin stability. Here we report a role for Synd in actin-regulated pseudocleavage furrow formation. Synd localized to these furrows, and its loss resulted in short, disorganized furrows. Synd presence was important for the recruitment of the septin Peanut and distribution of Diaphanous and F-actin at furrows. Synd and Peanut were both absent in furrow-initiation mutants of RhoGEF2 and Diaphanous and in furrow-progression mutants of Anillin. Synd overexpression in *rhogef2* mutants reversed its furrow-extension phenotypes, Peanut and Diaphanous recruitment, and F-actin organization. We conclude that Synd plays an important role in pseudocleavage furrow extension, and this role is also likely to be crucial in cleavage furrow formation during cell division.**

**Monitoring Editor**
Denise Montell
University of California, Santa Barbara

Received: Sep 18, 2015
Revised: Apr 25, 2016
Accepted: Apr 26, 2016

## INTRODUCTION

Cleavage furrow formation during cell division requires a highly conserved set of cytoskeletal and membrane-trafficking proteins (D'Avino, 2009; Haglund *et al.*, 2011; Cabernard, 2012; Fededa and Gerlich, 2012). Their positioning and initiation involves microtubules and the centralspindlin complex (Alsop and Zhang, 2003; Bringmann and Hyman, 2005; Crest *et al.*, 2012). Rho-GTPase–activating protein (RacGAP50C) of this complex positions Rho-GTP exchange factor (RhoGEF) Pebble at contractile rings, and another RhoGEF2 functions in pseudocleavage furrows to activate Rho1 for furrow initiation (Schmidt and Nichols, 2004; Buchsbaum, 2007). Rho1 recruits formins that assemble an actin scaffold for contractile-ring formation and/or furrow initiation (Barmchi *et al.*, 2005; Grosshans *et al.*, 2005; Watanabe *et al.*, 2008, 2010, 2013). Formin activity also depends on the presence of a scaffold protein, Anillin, at the contractile ring (Watanabe *et al.*, 2010; Saha and Pollard, 2012). RacGAP50C also accumulates Anillin at the furrow (D'Avino *et al.*, 2008; Gregory *et al.*, 2008), which is responsible for both septin and myosin II association at the contractile ring (Straight *et al.*, 2005; Piekny and Maddox, 2010). Cytokinesis failure increases in *Caenorhabditis elegans* when embryos are depleted of both Rho kinase and Anillin/septins (Maddox *et al.*, 2007), implying that they work together for robust furrow formation.

The cell division cycle is accompanied by drastic changes in cell shape that necessitate dynamic interplay between the membrane and actin cytoskeleton (Heng and Koh, 2010; Bezanilla *et al.*, 2015). In the *Drosophila* syncytial embryo, nuclear division cycles 10–13 are rapid and involve dynamic pseudocleavage furrow ingression and retraction between adjacent dividing nuclei. These furrows serve to prevent spindle cross-talk across compartments during metaphase of each cycle (Foe and Alberts, 1983; Kellogg *et al.*, 1988) and organize the embryo into discrete polarized functional units (Frescas *et al.*, 2006; Mavrakis *et al.*, 2009; Daniels *et al.*, 2012). Furrow

This article was published online ahead of print in MBoC in Press (http://www.molbiolcell.org/cgi/doi/10.1091/mbc.E15-09-0656) on May 4, 2016.

*Address correspondence to: Richa Rikhy (richa@iiserpune.ac.in).

Abbreviations used: Amph, Amphiphysin; ANOVA, analysis of variance; APC2, Adenomatous Polyposis Coli2; CytoD, cytochalasin D; Dia, Diaphanous; DMSO, dimethyl sulfoxide; FRAP, fluorescence recovery after photobleaching; FT, furrow tip; GFP, green fluorescent protein; Jasp, jasplakinolide; LatA, latrunculin A; MIP, maximum-intensity projection; N-Wasp, neuronal Wiscott-Aldrich syndrome protein; PBS, phosphate-buffered saline; PH, pleckstrin homology; RacGAP, Rho-GTPase–activating protein; RhoGEF, Rho-GTP exchange factor; ROI, region of interest.

positioning and initiation at this stage requires RhoGEF2 for recruiting Rho1 and the formin Diaphanous (Dia) (Barmchi *et al.*, 2005; Grosshans *et al.*, 2005; Crest *et al.*, 2012). Microtubules are required for furrow positioning (Bringmann and Hyman, 2005; Crest *et al.*, 2012), while furrow ingression involves dynamic growth of actin filaments through Profilin and the action of anticapping proteins (like Ena/VASP; Grevengoed *et al.*, 2003; Bezanilla *et al.*, 2015). The syncytial cycles are followed by massive elongation of furrows to form individual cells in a process called cellularization, during which membrane extension is fueled by flattening of apical microvilli and Rab11-mediated endocytosis (Lecuit and Wieschaus, 2000; Pelissier *et al.*, 2003; Figard *et al.*, 2013) and driven by an actomyosin contractile ring that, apart from actin and myosin II, also comprises Anillin, septins, RhoGEF2, and Dia (Lecuit, 2004; Royou *et al.*, 2004). Although contractile rings first form only during cellularization in early developing *Drosophila* embryos, the syncytial pseudocleavage furrows contain most of the proteins present in the contractile ring such as Rho1, RhoGEF2, Dia, Anillin, and septins (Fares *et al.*, 1995; Field and Alberts, 1995; Afshar *et al.*, 2000; Foe *et al.*, 2000; Cao *et al.*, 2008).

F-BAR domain–containing proteins link membrane and cytoskeleton in various processes, including endocytosis, cell shape and polarity, cell motility, and cytokinesis (Roberts-Galbraith and Gould, 2010; Liu *et al.*, 2015). The yeast orthologues of F-BAR protein Cip4 are known to recruit formins and influence their nucleation and elongation activities (Laporte *et al.*, 2011; Yan *et al.*, 2013; Graziano *et al.*, 2014; Willet *et al.*, 2015). In addition, Hof1 (Cip4 in *Saccharomyces cerevisiae*) coiled-coil domain binds Septin (Cdc10) and localizes it to the bud neck (Meitinger *et al.*, 2013; Oh *et al.*, 2013). *Drosophila* Cip4, however, is not essential for formin Dia recruitment to cellularization furrows, and its loss does not result in a defect in cellularization but its overexpression shows *dia* loss-of-function phenotypes (Yan *et al.*, 2013). The F-BAR domain protein, Syndapin/Pacsin (Synd), initially identified as a binding partner for Dynamin and neuronal Wiscott-Aldrich syndrome protein (N-Wasp) via its SH3 domain, participates in endocytosis and actin remodeling (Roos and Kelly, 1998; Simpson *et al.*, 1999; Qualmann and Kelly, 2000; Dharmalingam *et al.*, 2009; Rao *et al.*, 2010). Mammalian Synd1 binds to the actin nucleator Cordon bleu (Cobl) (Ahuja *et al.*, 2007) and mediates its interaction with Arp2/3 to affect actin nucleation during neuromorphogenesis (Schwintzer *et al.*, 2011). Synd, unlike other F-BAR proteins, directly binds and stabilizes F-actin (Kostan *et al.*, 2014) and, unlike any N- or F-BAR protein, can generate a range of membrane curvatures much greater than its own intrinsic curvature (Frost *et al.*, 2008; Ramesh *et al.*, 2013). *Drosophila* Synd promotes expansion of the subsynaptic reticulum (Kumar *et al.*, 2009b), which also requires actin-remodeling (Ramachandran *et al.*, 2009). *Drosophila* Synd also binds to Anillin via its myosin-binding domain in vitro, localizes at the cytokinetic furrow (earlier than *Drosophila* Cip4) in *D.Mel-2* cells, and is important for cytokinesis during male meiosis in primary spermatocytes (Takeda *et al.*, 2013). Together these studies suggest a role for Synd in coordinated membrane and actin remodeling during cleavage furrow formation. However, no analysis of its recruitment dynamics or functional analysis in organization of actin or actin-remodeling proteins with respect to furrow initiation or extension machinery has been carried out so far. In this study, we report that Synd is important for syncytial *Drosophila* pseudocleavage furrow extension; septin Peanut (Pnut) recruitment; and distinct Dia, Anillin, and actin localization. Most significantly, Synd can recruit actin remodeling proteins, organize actin, and result in furrow extension during pseudocleavage furrow formation in *rhogef2*-depleted embryos.

## RESULTS

### Synd is enriched at *Drosophila* syncytial pseudocleavage furrow tips

The nuclear division cycle from interphase through metaphase in the *Drosophila* syncytial embryo is accompanied by extension of the pseudocleavage furrow; the furrow being shortest in interphase and longest in metaphase, when mitotic spindles attach chromosomes at the equator (Figure 1A). An antibody generated against the Synd SH3 domain (Kumar *et al.*, 2009a,b) was used to study its localization in pseudocleavage furrows in wild-type syncytial *Drosophila* embryos (Figure 1B). We found that Synd localized to the apical and lateral membranes and was enriched at the furrow tip (FT), where it colocalized with Patj, a marker for the FT (Supplemental Figure S1A; Mavrakis *et al.*, 2009). Fluorescence intensity ratios of Synd to Amphiphysin (Amph, used as a membrane marker) were significantly reduced in embryos expressing *synd*$^{RNAi}$ (driven by *nanos*-Gal4) or containing a transposon in the first intronic region of the *synd* gene (*synd*$^{1d}$) (Kumar *et al.*, 2009a) in the *trans*-allelic combination of *synd*$^{1d}$/Df (Figure 1, C–E). *synd*$^{1d}$/Df had the highest embryo lethality at 24 h after egg deposition (Figure 1F), and we used this allelic combination for Synd depletion for all subsequent analyses. The antibody staining and lethality were rescued using the fluorescently tagged Ub-Syndapin::green fluorescent protein (Synd-GFP; Synd-GFP expressed with the ubiquitin promotor), indicating the functionality of this GFP-tagged Synd (Figure 1, B–D; Takeda *et al.*, 2013). The Synd-GFP localization overlaps almost completely with Synd antibody staining (Supplemental Figure S1B).

Synd distribution in metaphase furrows of nuclear cycles 11–13 was measured in living embryos expressing Synd-GFP in the *synd*$^{1d}$/Df background (Figure 1G and Supplemental Movie S3). Synd-GFP localized to the apical and lateral pseudocleavage furrow membranes and was progressively enriched at the FT in cycles 12 and 13 (Figure 1, G and H). This increase correlated with increase in furrow length with each nuclear cycle (Holly *et al.*, 2015). To assess Synd dynamics at the FT compared with the apical membrane, we used fluorescence recovery after photobleaching (FRAP) in these embryos during cycle 13 metaphase in the apical and FT membrane. The FRAP recovery data were fit to a one-phase exponential association equation (for diffusion-uncoupled FRAP); the recovery plateau obtained was higher at the metaphase FTs as compared with the apical region, with a mobile fraction of ~80% as compared with 60% (Figure 1, I–K). This difference of mobile fraction was not seen for the GFP-tagged pleckstrin homology (PH) domain of general receptor for phosphoinositides-1 (GRP1; tGPH; Britton *et al.*, 2002; Supplemental Figure S1, D and E). Thus Synd shows increased mobile fraction at the FTs in long metaphase furrows.

### *synd* mutants have shorter and disorganized pseudocleavage furrows

To study Synd's role in the dynamics of furrow formation, we imaged developing embryos containing tGPH as a plasma membrane marker to compare furrow lengths in orthogonal sections. We compared pseudocleavage furrow dynamics in control tGPH embryos at five time points in cycle 13: 1) end of prophase (prometaphase), when the nuclei are the largest and furrows start to ingress (3.8 ± 0.4 µm; denoted as I); 2) beginning of metaphase (after ~3 min), when the nuclear envelope breaks down (furrow length: 8.3 ± 0.6 µm; II); 3) middle of metaphase (III); 4) end of metaphase (~6 min), when the furrow is the longest (10.2 ± 0.8 µm; IV); and 5) anaphase, when the furrow starts to retract (~7 min; V) (Figure 2, A and B, and Supplemental Movie S1). The tGPH; *synd*$^{1d}$/Df furrows in prometaphase had a length similar to that of

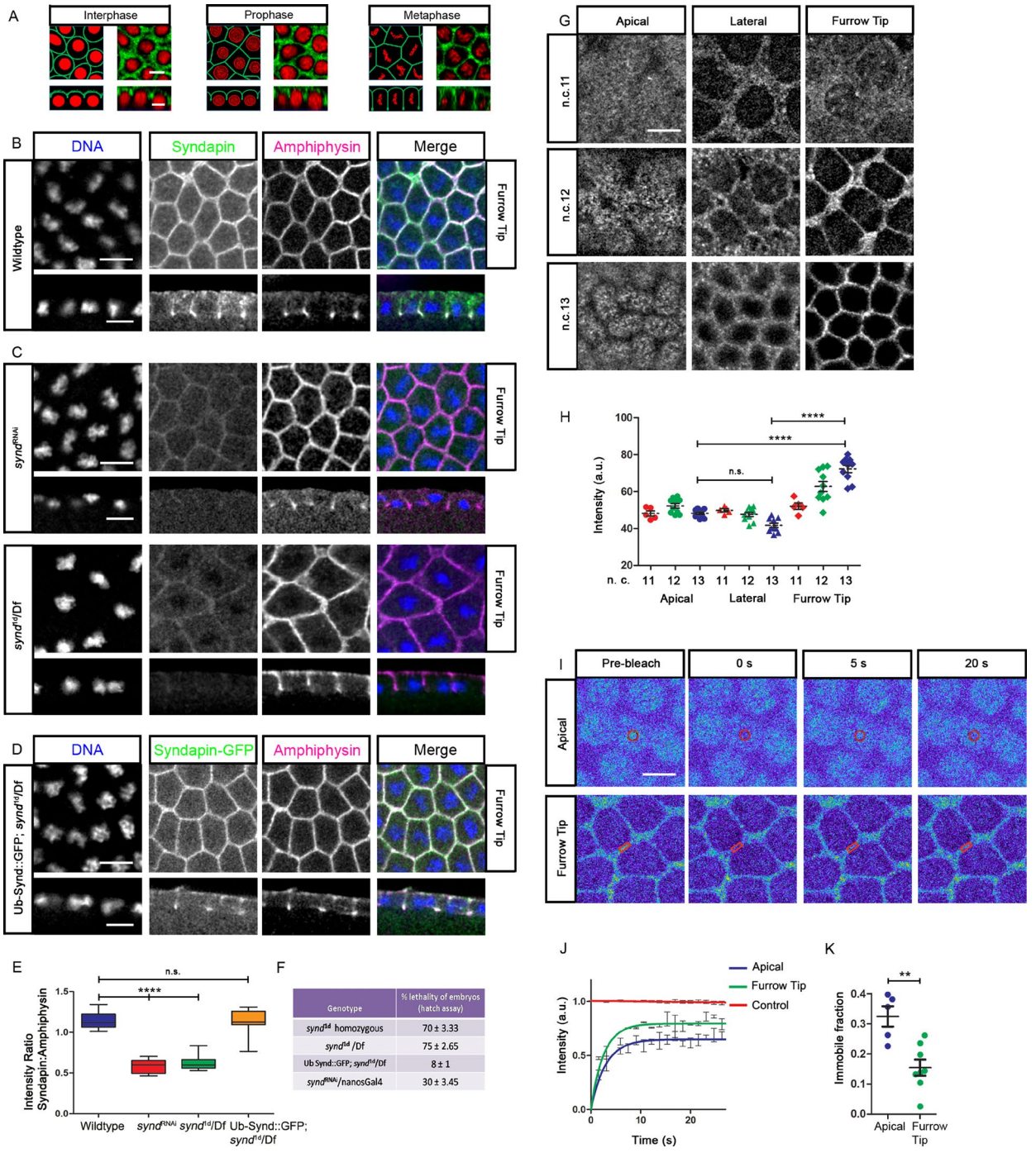


FIGURE 1: Synd is enriched at the pseudocleavage FT. (A) Pseudocleavage furrow extension visualized in syncytial nuclear cycle 13 with membrane marker Gap43-Venus (green) and histone-RFP (red). (B) Synd antibody/Synd-GFP (green) and Amph (magenta) are localized at metaphase (DNA, blue) furrow tip in wild-type embryos. (C–F) Synd immunostaining and embryo viability is reduced in mutants and rescued by Synd-GFP. Synd immunostaining ratio to Amph is reduced in *synd*$^{RNAi}$ (60%, $n = 15$) and *synd*$^{1d}$/Df (85%, $n = 40$) embryos in metaphase as compared with Synd-GFP (25%, $n = 16$) (C and D) and in a box plot using Syndapin:Amphiphysin fluorescence intensity ratios (E, $n = 3$; 15 furrows each, ****, $p < 0.0001$, n.s., not significant by nonparametric Mann-Whitney *U*-test). Mean ± SD of 24 h embryo lethality shows the highest lethality in *synd*$^{1d}$/Df, which is reversed by Synd-GFP ($n = 3$; 100 embryos/genotype), $p < 0.0001$ (F). (G and H) Synd FT association increases across syncytial cycles. Synd-GFP fluorescence in Synd-GFP; *synd*$^{1d}$/Df embryos in metaphase across nuclear cycles (n.c.) 11, 12, and 13 in the apical, lateral, and FT membranes (G) is quantified in a scatter plot (a.u., arbitrary units, $n = 3$; 10 membrane ROIs, ****, $p < 0.0001$, n.s. not significant, one-way ANOVA and Tukey's multiple-comparison test) (H). (I–K) Synd shows increased mobile fraction at the FT compared with the apical membrane. Photobleaching (black ROI, ~2.5 μm$^2$) of Synd-GFP was performed in apical or FT membranes; images at key time points are shown (I). FRAP occurs to a greater extent at the FT membrane ($n = 5$ embryos/region) (J). The immobile fraction from individual FRAP curves in H is shown in a scatter plot (K, $n = 5$; **, $p < 0.01$, nonparametric Mann-Whitney *U*-test). Scale bar: 10 μm.

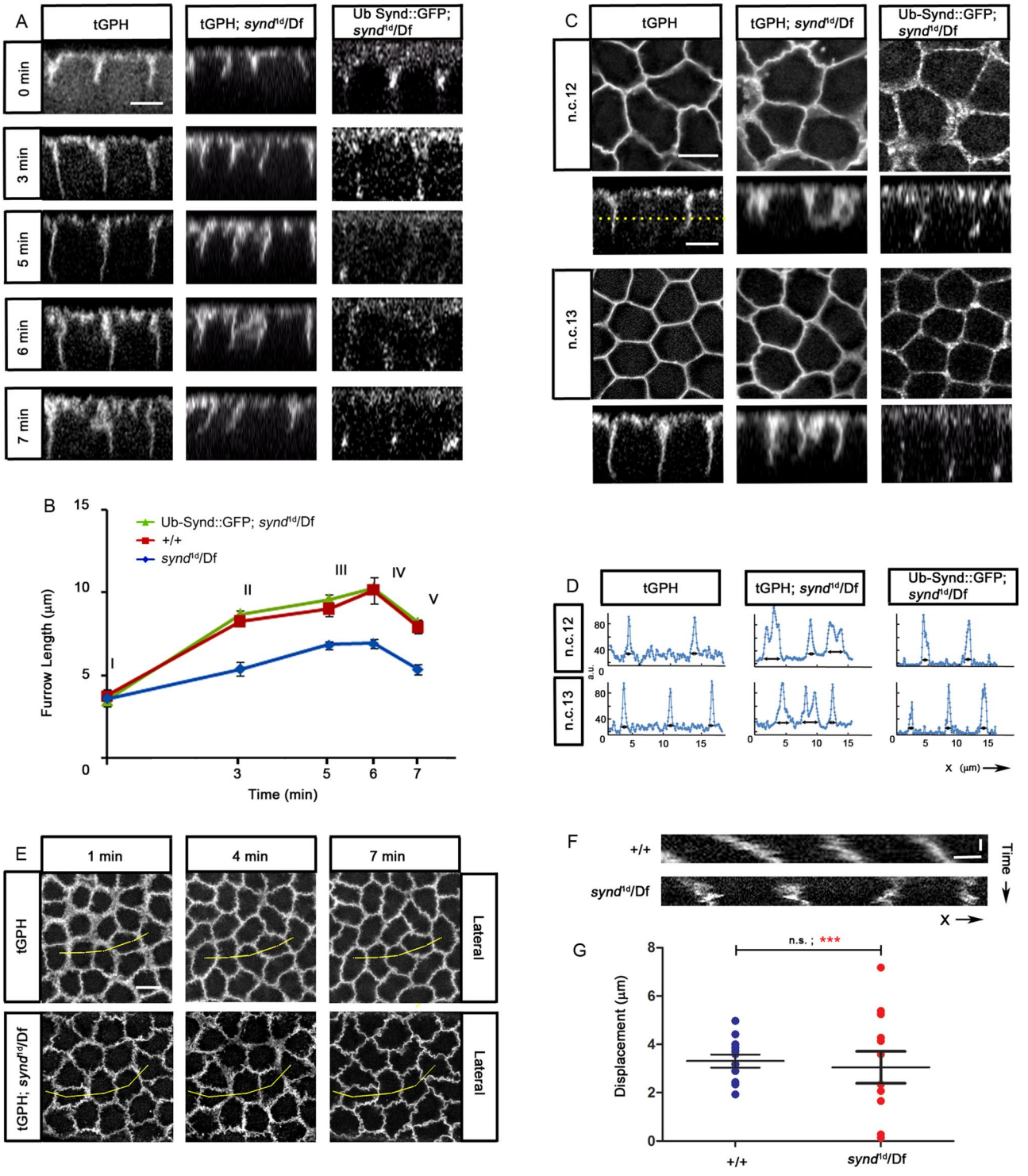


FIGURE 2: *synd* mutant embryos have short and disorganized pseudocleavage furrow membranes. (A and B) *synd* mutants have shorter metaphase furrow lengths. Time-lapse orthogonal views in tGPH control and *synd*$^{1d}$/Df embryos are shown at 0, 3, 5, 6, and 7 min (corresponding to I, II, III, IV, and V) in syncytial cycle 13 (A). Graph shows significantly decreased furrow lengths in *synd*$^{1d}$/Df (B, mean ± SEM, $n = 3$; 5 furrows/embryo). (C and D) *synd* mutants have loosened metaphase furrow membranes. Surface and orthogonal views of longest metaphase furrows from tGPH expressing control, *synd*$^{1d}$/Df, and Synd-GFP; *synd*$^{1d}$/Df embryos in cycles 12 and 13 (C). *synd*$^{1d}$/Df embryos show increased width (arrows) in Line scan-intensity profile across lateral furrow membranes compared with control and Synd-GFP–expressing embryos (D). (E–G) *synd* mutants have decreased *x,y* displacement in the syncytial cycle. Time-lapse surface views are shown at ~1, 4, and 7 min from tGPH containing control and *synd*$^{1d}$/Df embryos in cycle 13 (yellow line indicates track selected for kymograph generation) (E and F). The average displacement in a scatter plot is not significantly different ($n = 3$; 4 furrows/embryo, $p > 0.05$, n.s., not significant) but variance is increased in *synd*$^{1d}$/Df (G). ****, $p < 0.0001$, *F*-test used to compare variances. Unpaired *t* test (two-tailed) with Welch's correction used to compare means. Scale bar: 10 µm; kymograph scale bar: $x = 2.5$ µm; $y = 100$ s.

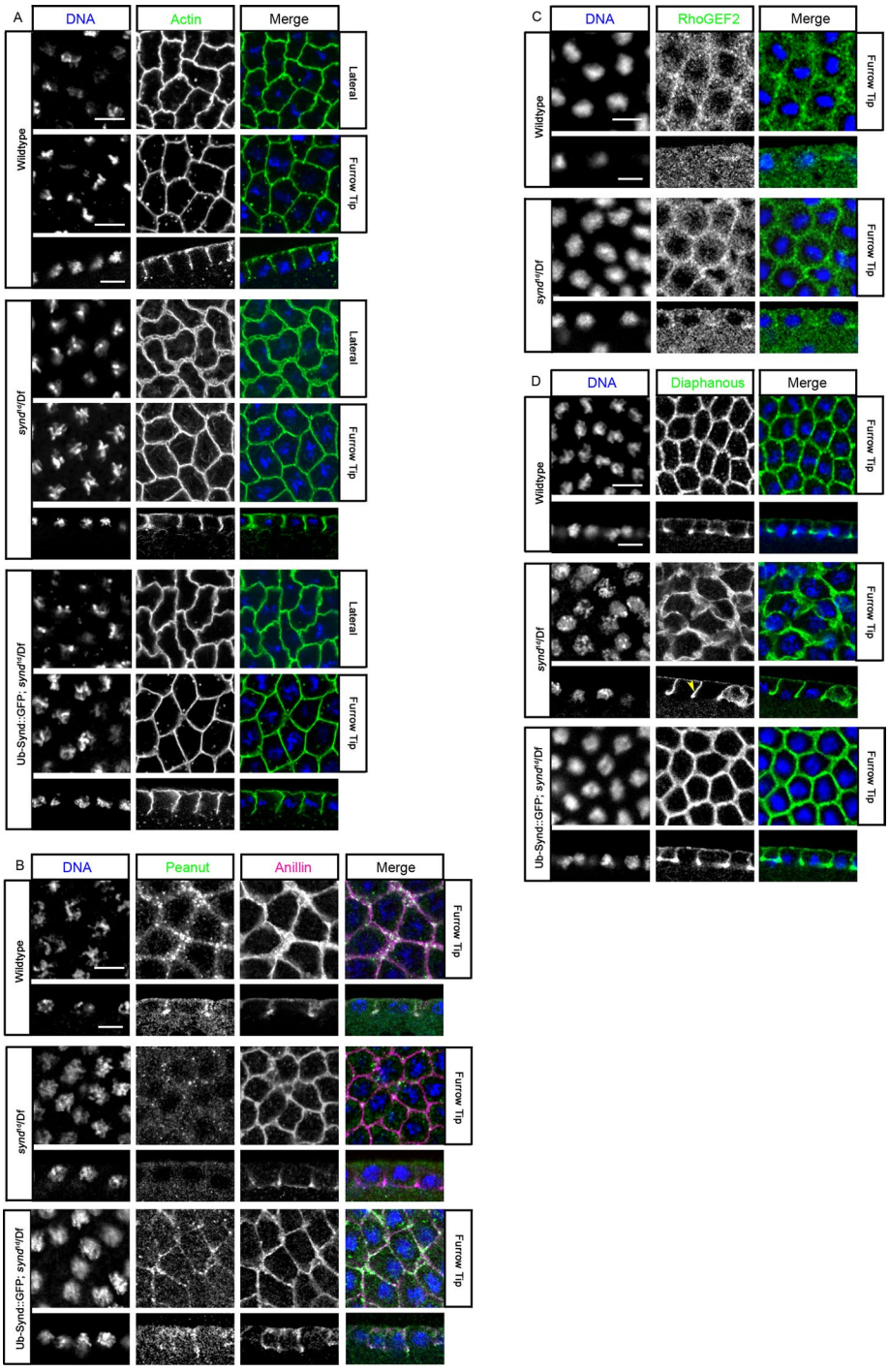


FIGURE 3: *synd* mutant embryos show Pnut loss from pseudocleavage furrow membranes. (A) F-actin distribution (green) in *synd*$^{1d}$/Df reveals loose membrane and absence of F-actin puncta below cortex (77%, $n = 33$) compared with wild-type (3%, $n = 50$) and Synd-GFP; *synd*$^{1d}$/Df (25%, $n = 16$) embryos. (B) *synd*$^{1d}$/Df embryos show Pnut (green) loss (93%, $n = 44$) as compared with wild type (2%, $n = 45$) and Synd-GFP; *synd*$^{1d}$/Df (30%, $n = 14$). Anillin localizes normally to the furrow tip membrane (magenta) (86%, $n = 44$) in metaphase. (C) RhoGEF2 (green) antibody distribution is unchanged in *synd*$^{1d}$/Df (91%, $n = 11$) compared with wild-type embryos. (D) Dia (green) is uniformly distributed along the furrow membrane in *synd*$^{1d}$/Df (90%, $n = 50$) compared with wild-type (3%, $N = 50$) and Synd-GFP; *synd*$^{1d}$/Df (25%, $n = 16$) embryos. Yellow arrow indicates uniform Dia staining along length of furrow (D); scale bar is for all panels in A–D. Scale bars: 10 μm.

the control (3.6 ± 0.5 μm); however, their length remained constant through metaphase (6.8 ± 0.5 μm) and was significantly shorter than that of the control. The anaphase furrow (5.4 ± 0.3 μm) was also much shorter than that of the control (7.9 ± 0.4 μm) at 7 min. These furrow extension–retraction dynamics were rescued in *synd* mutant embryos containing Synd-GFP (Figure 2, A and B, and Supplemental Movies S2 and S3). We found that furrow dynamics measured in embryos expressing different PH domains (tGPH, PHPLCδ-CFP) and in Synd-GFP; *synd*$^{1d}$/Df embryos were indistinguishable from each other (unpublished data).

The furrow membrane in Synd-depleted embryos appeared "loosened" or ruffled as compared with a sharp, distinct furrow in tGPH and Synd-GFP; *synd*$^{1d}$/Df rescue embryos (Figure 2, C and D). This was depicted with a line scan across the metaphase lateral furrow membrane that revealed broader peaks in cycles 12 and 13 in mutant embryos as compared with focused peaks in tGPH and rescue embryos. The furrow plasma membrane moves laterally and synchronously in the *x,y* plane during the syncytial cycles, and we reasoned that this displacement will be affected if the furrow membranes are shorter and loosened. Previous studies in *Xenopus* embryos have also shown that loose membranes in planar cell polarity and septin mutants during collective cell migration exhibited increased undulating behavior in kymographs (Kim *et al.*, 2010). A plot of the mean syncytial furrow-membrane displacement showed a significantly higher variance in *synd*-depleted embryos as compared with control. Also, the displacement of adjacent furrows occurred asynchronously in mutant embryos (Figure 2, F and G). Thus Synd is required for appropriate furrow elongation, and its deficiency not only causes defects in furrow extension but also membrane ruffling and correlates with an altered displacement and asynchrony in lateral membrane movement.

### *synd* mutants show a loss of Pnut and mislocalization of Dia on the pseudocleavage furrow

Defects in furrow extension prompted us to check the effect of *synd* mutant on key players of cleavage furrow initiation/extension. Because actin remodeling is likely to be the main downstream driver of furrow ingression in the syncytial embryo (Webb *et al.*, 2009), and Synd can directly bind and stabilize actin (Kostan *et al.*, 2014), we first used fluorescent phalloidin to check F-actin levels and distribution (Figure 3A). F-actin levels were unaffected in *synd* embryos. However, F-actin staining also revealed "looseness" in the lateral furrow membrane as shown by tGPH (Figure 2), and this was rescued with Synd-GFP.

The short-furrow phenotype of *synd* mutant embryos phenotypically mimics *anillin* mutants that fail to recruit Pnut on furrow membranes (Silverman-Gavrila *et al.*, 2008). Anillin recruits Pnut to the membrane via its PH domain (Oegema *et al.*, 2000; Field *et al.*, 2005; Liu *et al.*, 2012; Kinoshita *et al.*, 2015) and promotes stable intercellular bridge elongation before abscission (Renshaw *et al.*, 2014). Pnut organizes actin into bundles at highly curved geometries like those in furrow canals during cellularization (Mavrakis *et al.*, 2014). We thus looked at the effect of *synd* mutant on Pnut and Anillin in the syncytial embryo. Interestingly, we found that, in *synd* mutant embryos, Pnut association with the pseudocleavage furrow membrane was lost, a defect that was partially reversed by expression of Synd-GFP transgene (Figure 3B). However, Anillin was present on the furrow tip in *synd*$^{1d}$/Df embryos (Figure 3D). Taken together, this suggests that Pnut recruitment to the membrane does not depend only on its binding to Anillin, but also on Synd and the Anillin-Synd-Pnut interaction is significant for pseudocleavage furrow formation.

Missing and short furrows are caused due to the absence of RhoGEF2 and Dia during syncytial divisions and cellularization (Afshar *et al.*, 2000; Barmchi *et al.*, 2005), implicating them in furrow initiation and extension. In syncytial embryos, RhoGEF2 is cytoplasmic in interphase and localizes to FTs in prophase (Barmchi *et al.*, 2005). Rho1, the downstream RhoGTPase effector of RhoGEF2, is required for Dia recruitment to cellularizing furrows (Grosshans *et al.*, 2005); however, there may be other RhoGEF2-independent mechanisms for Rho1 activation (Yoshida *et al.*, 2009) that allow some Dia to still be recruited to the membrane in germ-line clone *rhogef2* mutants (Supplemental Figure S2A and Supplemental Table S1) or RhoGTPase-independent mechanisms may be implicated in its recruitment (Yonetani *et al.*, 2008; Ang *et al.*, 2010). RhoGEF2 was unaffected in *synd* mutant embryos and localized to the metaphase furrow (Figure 3C), showing that Synd presence on the furrow membrane is not important for RhoGEF2 recruitment.

Dia was identified as a gene responsible for cytokinesis (Castrillon and Wasserman, 1994). It initiates furrow formation along with Adenomatous Polyposis Coli2 (APC2) in *Drosophila* syncytial embryos (Webb *et al.*, 2009), and Dia and APC1 collaborate to increase actin nucleation (Jaiswal *et al.*, 2013). In *synd*$^{1d}$/Df embryos, Dia was present uniformly along the length of the furrow in sagittal views, unlike in wild type, where it was enriched at the FT. Dia enrichment at furrow tips was rescued with Synd-GFP (Figure 3D). Altogether we observed that, in *synd* mutants, Pnut was completely depleted from the furrow, while F-actin, Anillin, and Dia were present on the furrow membrane. These data suggest that Synd contributes to stable furrow formation by recruitment of Pnut and enrichment of Dia at the FT.

### RhoGEF2, Dia, Anillin, and Pnut are each necessary for the recruitment of Synd on the *Drosophila* syncytial pseudocleavage furrow

Conversely, to test whether Synd recruitment depends on presence of proteins known to affect furrow formation, we imaged germ-line clone mutant embryos and/or RNA interference (RNAi) lines for *rhogef2*, *dia*, *anillin*, and *pnut* for Synd antibody localization and found that they are defective for localization of Synd (Figure 4, A and B). Each of these mutants also showed an apical accumulation of F-actin (Figure 4, A and B, Supplemental Figure S2, A and B, and Supplemental Table S1). Most interestingly, these mutants showed significantly reduced Pnut, implying a strong correlation between Synd and Pnut localization on the membrane (Supplemental Figure S2, A and B, and Supplemental Table S1). *dia*$^{5}$ mutant embryos also showed a loss of Anillin and Pnut, as reported previously (Afshar *et al.*, 2000), and *anillin* mutants in turn showed reduced levels of Dia (Supplemental Figure S2 and Supplemental Table S1). In *pnut* mutant embryos, Anillin was present, but levels were reduced on furrows (Supplemental Figure S2 and Supplemental Table S1). These observations together corroborate the role of Dia in Anillin and Pnut recruitment and also of Anillin in Pnut recruitment.

Because Synd was depleted in *pnut* mutants, Pnut was in turn depleted in *synd* (Supplemental Figure S2, A and B, and Supplemental Table S1), and Dia has been shown to be important for furrow initiation (Grosshans *et al.*, 2005), we doubly depleted *pnut* and *dia* in *synd* mutants by combining *pnut*$^{XP}$ and *dia*$^{5}$ alleles in one copy each (heterozygous) with *synd*$^{1d}$/Df to see whether the defects intensified. In each case, we obtained very few embryos, suggesting an increased severity as compared with *synd*$^{1d}$/Df, *dia*$^{5}$/+, and *pnut*$^{XP}$/+. Phalloidin revealed stronger defects, such as broader FTs in *pnut*$^{XP}$/+; *synd*$^{1d}$/Df and missing furrows in *dia*$^{5}$/+; *synd*$^{1d}$/Df that have been previously observed in *dia*$^{5}$ germ-line mutants (Figure 4, A and B; Afshar *et al.*, 2000; Grosshans *et al.*, 2005). Thus the furrow phenotype of *synd*$^{1d}$/Df was worsened by doubly depleting Dia or Pnut.

### Defects in pseudocleavage furrow extension and morphology in *rhogef2*$^{RNAi}$ are reversed by Synd overexpression

Because furrow-initiation/extension dynamics in *pnut* and *rhogef2* mutant embryos are uncharacterized, we studied this in tGPH-containing embryos depleted for Pnut and RhoGEF2 and found that they phenocopied *synd*$^{1d}$/Df embryos; the furrow length at 6 min (IV, when the furrow is the longest) was reduced compared with controls (Figure 5, A and B, and Supplemental Movies S4–S6). The *pnut*$^{XP}$/+; *synd*$^{1d}$/*synd*$^{1d}$ combination had short furrows (II–IV) like *synd*$^{1d}$/Df embryos. To check whether Synd and Pnut can promote furrow dynamics in the absence of RhoGEF2, we overexpressed Synd and Pnut in the *rhoGEF2*$^{RNAi}$ background. A combination of Synd-GFP with *rhoGEF2*$^{RNAi}$ showed a rescue (IV), and the furrows were longer than those observed in either tGPH or Synd-GFP; *synd*$^{1d}$/Df embryos alone (I–III and V; Figure 5, A and B, Supplemental Figure 2B, and Supplemental Movie S7). Overexpression of Pnut in the *rhoGEF2*$^{RNAi}$ background, however, did not abrogate the furrow length or loosened membrane phenotypes (Supplemental Figure S3, A–H). This shows that Synd could specifically rescue furrow extension in *rhoGEF2*$^{RNAi}$-expressing embryos.

Like *synd* mutant embryos, *rhogef2*$^{RNAi}$ and *pnut*$^{RNAi}$ mutant embryos had broad furrows and loosening of membrane along the edges revealed by a line scan across orthogonal sections in cycles 12 and 13 (Figure 5, C and D). Multiple kymograph analyses for lateral furrow membrane in the *x,y* plane showed significantly less mean displacement and therefore increased severity in *rhogef2*$^{RNAi}$, *pnut*$^{RNAi}$, and *pnut*$^{XP}$/+; *synd*$^{1d}$ combination mutants as compared with *synd*$^{1d}$/Df (Figure 5G and Supplemental Figure 2G). Furrow displacement depends on Rhogef2 and Pnut, and *synd* mutant embryos show a significant defect in displacement along with lowering of Pnut in the *pnut*$^{XP}$/+ background.

In summary, we found that *pnut* and *rhogef2* mutant embryos phenocopied the furrow-extension defects of *synd* mutant embryos and Synd overexpression could reverse the furrow defects in *rhogef2* mutant embryos.

### Rab5 early endosome depletion in *rhogef2* mutant embryos is not reversed by Synd overexpression

Synd functions in Clathrin/Dynamin-mediated endocytosis and actin remodeling (Qualmann and Kelly, 2000; Edeling *et al.*, 2009).

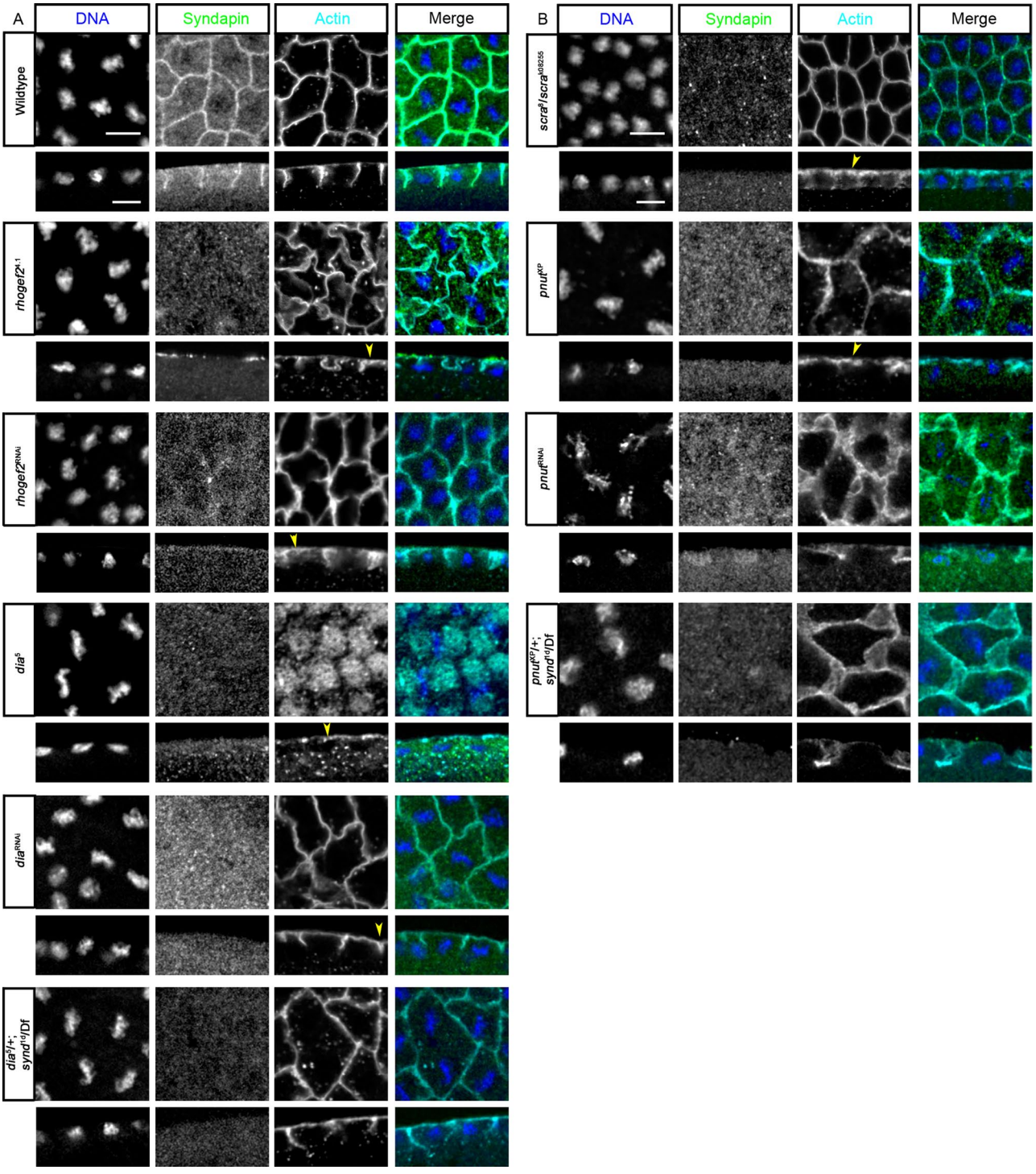


FIGURE 4: *rhogef2*, *dia*, *anillin*, and *pnut* mutant embryos show Synd loss from pseudocleavage furrow membranes. (A and B) Synd (green) immunostaining is lost in mutants for *rhogef2* (*rhogef2*$^{4.1}$; 88%, $n = 14$) and *rhogef*$^{RNAi}$ (87.5%, $n = 16$), *dia* (*dia*$^{5}$; 100%, $n = 15$) and *dia*$^{RNAi}$ (50%, $n = 20$), and in *dia*$^{5}$/+; *synd*$^{1d}$/Df (100%, $n = 10$) (A), *anillin* (*scra*$^{8}$/*scra*$^{k08255}$) (100%, $n = 14$), *pnut* (*pnut*$^{XP}$ (99%, $n = 22$), *pnut*$^{RNAi}$ (44%, $n = 18$), and *pnut*$^{XP}$/+; *synd*$^{1d}$/Df (91%, $n = 11$) (B) compared with wild type in metaphase furrows (DNA, blue). Yellow arrow indicates apical actin accumulation. Scale bars: 10 μm.

Therefore we evaluated the contribution of Synd's role in endocytosis for metaphase furrow formation. First we analyzed the localization of Dynamin/Shibire in *synd*$^{1d}$/Df embryos. Dynamin levels in immunostained *synd* mutant embryos were unaffected and colocalized with Amph at the furrow tip. *rhogef2*$^{RNAi}$ showed a punctate distribution of Dynamin similar to that seen in *shi*$^{RNAi}$ (Figure 6A). *shi*$^{ts}$ embryos also showed reduced Synd distribution on the membrane (Figure 6B) that correlated with previously observed reduction in Pnut levels and loss of metaphase furrow formation (Rikhy *et al.*, 2015).

Endocytosis occurs at the tip of the ingressing syncytial furrows and can be visualized in the form of tubules labeled with Amph (Sokac and Wieschaus, 2008a). Their formation depends on actin and Dynamin and correlates with the rate of furrow ingression in cellularization (Oegema *et al.*, 2000; Sokac and Wieschaus, 2008a, 2008b; Su *et al.*, 2013). We quantified the length of tubules in control and mutant embryos. *synd*$^{1d}$/Df embryos showed a significant decrease in length of tubules (Supplemental Figure S4, A and B). Synd-GFP expression in *synd*$^{1d}$/Df embryos restored the tubule length defect comparable to wild type. *shi*$^{ts}$ mutant embryos at the restrictive temperature are reported to show an increase in length of tubules during cellularization (Sokac and Wieschaus, 2008a; Su *et al.*, 2013); we also found a significant increase in their length compared with wild type in syncytial cycles (Supplemental Figure S4, A–C). In *rhogef2*$^{RNAi}$ embryos, there was no significant change in the tubule length. When Synd-GFP was overexpressed in *rhogef2*$^{RNAi}$ embryos, the tubule length increased slightly (Supplemental Figure S4, A–C). Rab5 early endosome vesicles increase when *shi*$^{ts2}$ embryos are released from the temperature-sensitive block (Rikhy *et al.*, 2015). We found that the number of Rab5 punctae were significantly lowered in *synd* mutant and *rhogef2*$^{RNAi}$ embryos compared with wild-type and phenocopied *shi*$^{ts}$ embryos at the restrictive temperature. Rab5 vesicle numbers were rescued upon overexpression of Synd-GFP in *synd* mutant but not in *rhogef2* mutant embryos (Figure 6, C and D). Taken together, these data indicate that Synd-GFP expression rescued the Amph tubule length defect and Rab5 vesicle number in *synd* mutant embryos but did not rescue the Rab5 vesicle number in *rhogef2* mutant embryos.

### Defects in recruitment of Pnut in *rhogef*$^{RNAi}$ are partially reversed by Synd overexpression

Finally, we analyzed the localization of Dia, Anillin, Pnut, and F-actin to the pseudocleavage furrow membrane in *rhogef2*$^{RNAi}$ embryos alone and with Synd overexpression (Figure 7, A–D). On overexpression with Synd-GFP in the *rhogef2*$^{RNAi}$ background, we observed a rescue in Dia and Pnut localization to the pseudocleavage furrow membrane compared with *rhogef2*$^{RNAi}$ embryos (Figure 7, A and B). F-actin localization to furrows was uniform, and its apical accumulation was lost (Figure 7C). To gain further insight into morphological defects in F-actin seen in *rhogef2* and *synd* mutants, we used structured illumination by Airyscan and three-dimensional (3D) surface rendering. The maximum-intensity projection (MIP) and surface-rendered image (Surface) in wild type revealed long and short actin along with few punctate structures. In *synd* mutants, however, the long structures were lost, and F-actin was disorganized and punctate along the furrow. Likewise, in *rhogef2*$^{RNAi}$, actin was accumulated in disorganized patches, and there were no long structures. On overexpression of Synd-GFP in the *rhogef2*$^{RNAi}$ background, we found long, organized actin with fewer puncta. Even though this organization was not exactly as in the wild-type furrow (there were mostly longer structures and very few short structures), it allowed actin to grow into elongated structures that could restore furrow length (Figure 7D). Thus Synd is important for organizing F-actin into more continuous structures at the furrow and can, in the process, rescue furrow phenotypes in *rhogef2* mutants.

To independently test whether actin stabilization can directly promote furrow actin organization, we analyzed the effects of the actin-binding drugs Jasplakinolide (Jasp), Cytochalasin D (CytoD), and Latrunculin A (LatA) on *synd* and *rhogef2*$^{RNAi}$ embryos. LatA binds to monomeric actin and prevents it from polymerizing into filaments, thereby rapidly disrupting the actin cytoskeleton (Coué *et al.*, 1987). LatA treatment resulted in drastic disruption of actin structures, with F-actin either only in caps or in very short furrows in both wild-type and mutant embryos (Supplemental Figure S3J). Jasp acts by markedly enhancing rates of actin polymerization and stabilizes actin filaments in vitro (Bubb *et al.*, 1994, 2000). On treatment with Jasp, *synd* mutant embryos showed fewer puncta on the membrane, and both *synd* and *rhogef2* embryos showed more organized actin structures and disorganized furrows (Figure 7E). This is consistent with in vivo studies that suggest that Jasp promotes de novo nucleation resulting in disordered polymeric actin and insufficient monomeric actin for remodeling of stress fibers (Bubb *et al.*, 2000; Ou *et al.*, 2002). CytoD, on the other hand, binds and prevents growth at the barbed ends of actin filaments, potentially allowing growth at the pointed end, which elongates more slowly (Carlier *et al.*, 1986). Reports suggest that cytochalasins have greater nucleating and bundling properties when actin networks are relatively labile, as in wounded/mutant cells (Goddette and Frieden, 1986), and disruption of actin allows CytoD to reorganize it into thick networks (Foissner and Wasteneys, 1999) or stable rods (Collings *et al.*, 1995) in a concentration-dependent manner (Foissner and Wasteneys, 2000). CytoD treatment caused continuous structures of actin to form and was able to form elongated furrows in *synd* and *rhogef2* mutant embryos compared with dimethyl sulfoxide (DMSO) control (Figure 7E). However, at twice this concentration, actin was disorganized and disrupted in wild-type embryos (Supplemental Figure S3I). Thus we can confirm that reorganizing actin into continuous structures can restore furrow actin organization and morphology in *synd* and *rhogef2* mutant embryos.

## DISCUSSION

Syndapins belong to the family of highly conserved F-BAR–domain containing proteins with diverse roles in membrane tubulation (Kumar *et al.*, 2009a; Ramesh *et al.*, 2013), Clathrin-mediated and bulk endocytosis (Qualmann *et al.*, 1999; Qualmann and Kelly, 2000), and actin remodeling (Qualmann *et al.*, 1999; Qualmann and Kelly, 2000; de Kreuk *et al.*, 2011; Kostan *et al.*, 2014) and cytokinesis (Takeda *et al.*, 2013). Synd is thus poised to play a role in processes like furrow formation, which need orchestrated remodeling of both the membrane and the cytoskeleton (Bezanilla *et al.*, 2015). Furrow elongation in syncytial *Drosophila* embryos is an excellent model system to study the role of proteins that drive its formation. Previous studies show that furrow formation involves membrane addition by trafficking and membrane extension by remodeling of the actin meshwork (Afshar *et al.*, 2000; Stevenson *et al.*, 2002; Cao *et al.*, 2008; Crest *et al.*, 2012; Figard *et al.*, 2013; Holly *et al.*, 2015; Rikhy *et al.*, 2015). We have been able to conclusively demonstrate that Synd functions to promote furrow formation by organization and elongation of F-actin structures (Figure 8). We show that Synd is essential for recruitment and distribution of Pnut and Dia on the membrane (Figure 3). In turn, Pnut and Dia also affect Synd distribution on the membrane (Figure 4). RhoGEF2/Dia and Anillin/Pnut have been previously shown to regulate F-actin architecture at cleavage and cellularization furrows (Afshar *et al.*, 2000; Liu *et al.*, 2012; Mavrakis *et al.*, 2014), and loss of Synd in *synd* mutants therefore affects actin both directly and through its influence on Pnut and Dia localization. As with other actin-regulated processes, even though a linear pathway of association/regulation of these actin-remodeling proteins to the furrow membrane is unlikely, our data imply that Synd is a key component in the RhoGEF2-Dia-Anillin/Pnut pathway during actin-driven furrow elongation. Synd2 can bind and inhibit Rac1 via its SH3 domain, thus reducing Arp2/3 activity (de Kreuk *et al.*, 2011), and may therefore be able to potentiate Dia

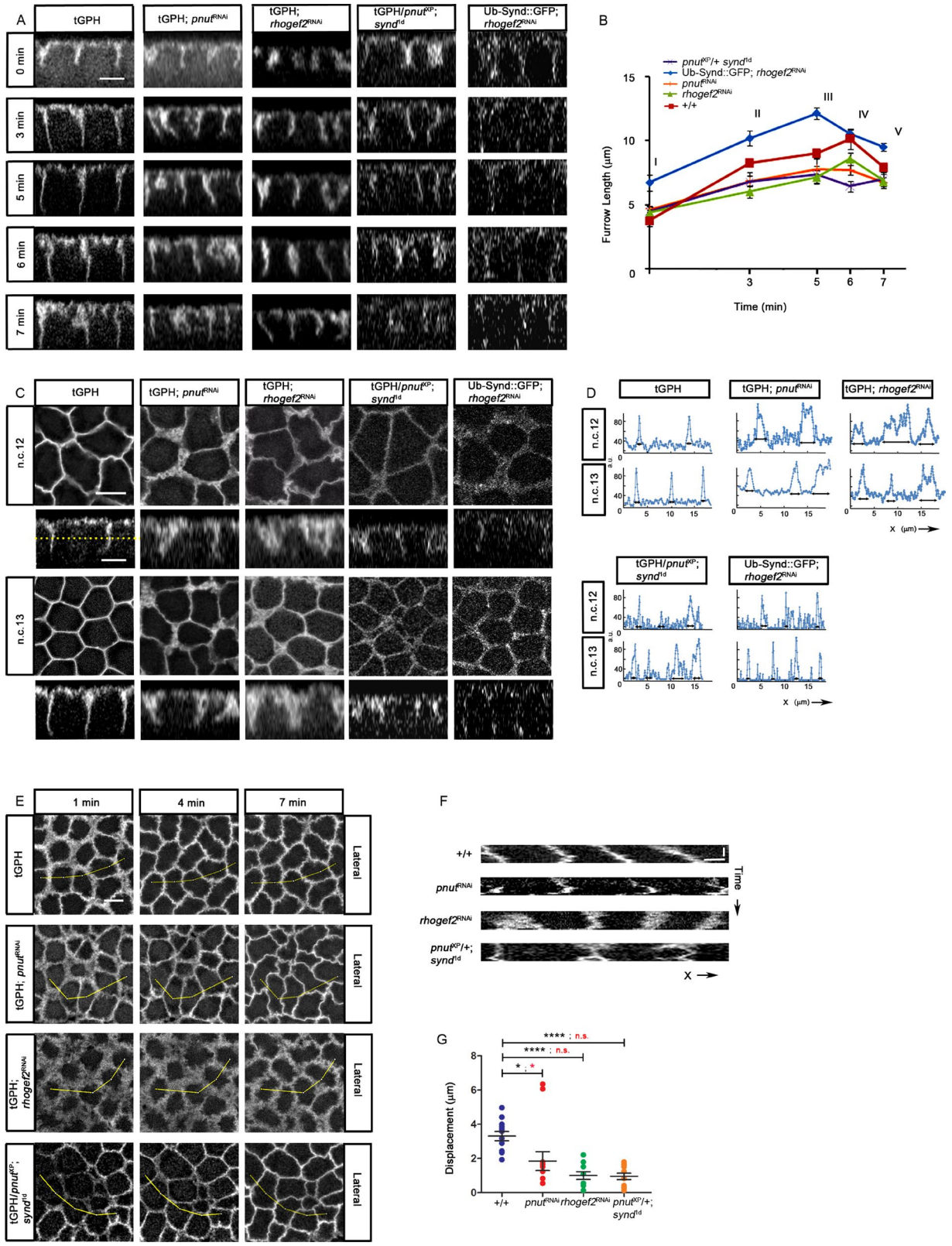


FIGURE 5: Aberrant furrow membrane phenotype and Pnut recruitment in *rhogef2*$^{RNAi}$ embryos is reversed by Synd overexpression. (A–G) *pnut* and *rhogef2* mutant embryos have decreased metaphase furrow lengths, loose furrow membranes, and decreased *x,y* displacement, and *rhogef2*$^{RNAi}$ phenotypes are reversed by Synd-GFP. Time-lapse orthogonal views (A) at 0, 3, 5, 6, and 7 min (corresponding to I, II, III, IV, and V) of furrow extension in *pnut*$^{RNAi}$, *rhogef2*$^{RNAi}$, and *pnut*$^{XP}$/+; *synd*$^{1d}$ mutants expressing tGPH show a decrease compared with control and Synd-GFP; *rhogef2*$^{RNAi}$ (B) (mean ± SEM) ($n = 3$; 5 furrows/embryo). Surface and orthogonal views of longest metaphase furrows in *pnut*$^{RNAi}$, *rhogef2*$^{RNAi}$, and *pnut*$^{XP}$/+; *synd*$^{1d}$ compared with control and Synd-GFP; *rhogef2*$^{RNAi}$ embryos in nuclear cycles 12 and 13 (C). Line scan-intensity profile across mutant furrow membranes shows a broader area (arrows) that is

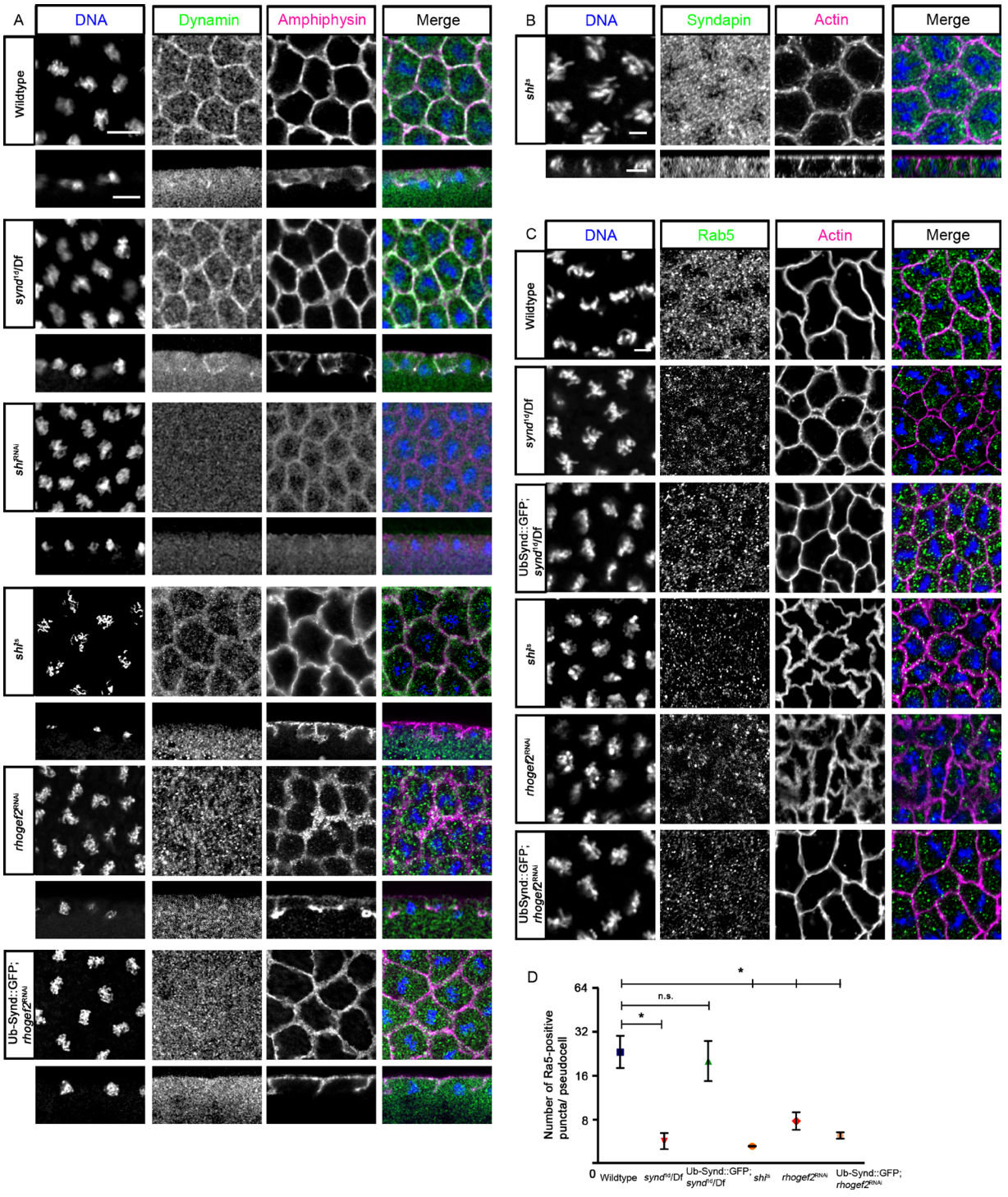


FIGURE 6: Rab5 early endosomes are depleted in *synd* and *rhogef2*$^{RNAi}$ embryos. (A) Dynamin (green) distribution is unaffected in *synd* mutant embryos. Dynamin levels are unaffected in *synd*$^{1d}$/Df embryos but have a punctate distribution in *shi*$^{RNAi}$, *shi*$^{ts}$, *rhogef2*$^{RNAi}$, and Synd-GFP; *rhogef2*$^{RNAi}$ embryos (100%, $n = 10$) compared with wild type. (B) Synd is reduced from the furrow membrane in *shi*$^{ts}$ embryos (100%, $n = 12$). (C and D) Rab5 vesicle immunostaining and numbers/pseudocell are decreased in *synd*$^{1d}$/Df, *shi*$^{ts}$, and *rhogef2*$^{RNAi}$. Rab5 vesicle numbers are rescued in Synd-GFP; *synd*$^{1d}$/Df and not in Synd-GFP; *rhogef2*$^{RNAi}$ embryos ($n = 3$, n.s., not significant, *, $p < 0.05$, nonparametric Mann-Whitney *U*-test).

reversed in the Synd-GFP; *rhogef2*$^{RNAi}$ (D). Time-lapse surface views (E) at ~1, 4, and 7 min of lateral membranes from tGPH containing *pnut*$^{RNAi}$, *rhogef2*$^{RNAi}$, tGPH/*pnut*$^{XP}$; *synd*$^{1d}$ show less displacement (across the yellow line) in the *x,y* plane compared with control embryos in cycles 13 (F and G) ($n = 3$; 4 furrows/embryo, *, $p < 0.05$, ****, $p < 0.0001$, unpaired *t* test [two-tailed] with Welch's correction, variance: n.s., not significant, *, $p < 0.05$, *F*-test to compare variances). Scale bars: 10 µm; kymograph scale bar: $x = 2.5$ µm; $y = 100$ s.

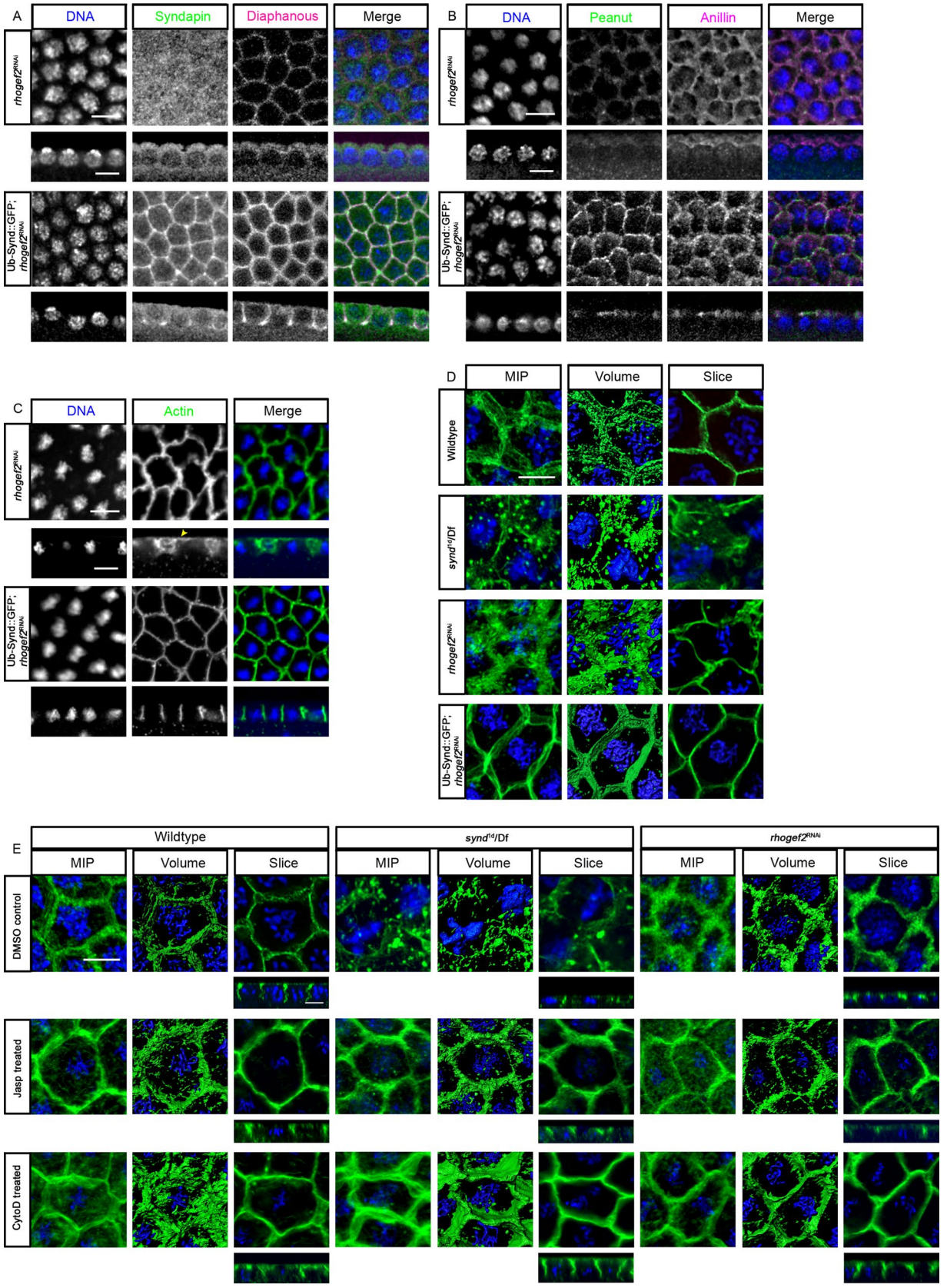


FIGURE 7: Synd overexpression reverses the actin organization and actin remodeling protein recruitment defects in *rhogef2*$^{RNAi}$ mutant embryos. (A–D) Dia, Anillin, and Pnut recruitment defects in *rhogef2*$^{RNAi}$ are reversed by Synd-GFP. Synd-GFP; *rhogef2*$^{RNAi}$ metaphase (DNA, blue) embryos show a reversion of Dia (magenta) (50%, $n = 10$ compared with 91%, $n = 22$ in *rhogef2*$^{RNAi}$) (A), Pnut (green) and Anillin (magenta; 66%, $n = 12$ compared with 100%, $n = 14$ in *rhogef2*$^{RNAi}$) (B) apical accumulation of actin (green) (50%, $n = 10$ compared with 100%, $n = 16$ in *rhogef2*$^{RNAi}$) (C). F-actin

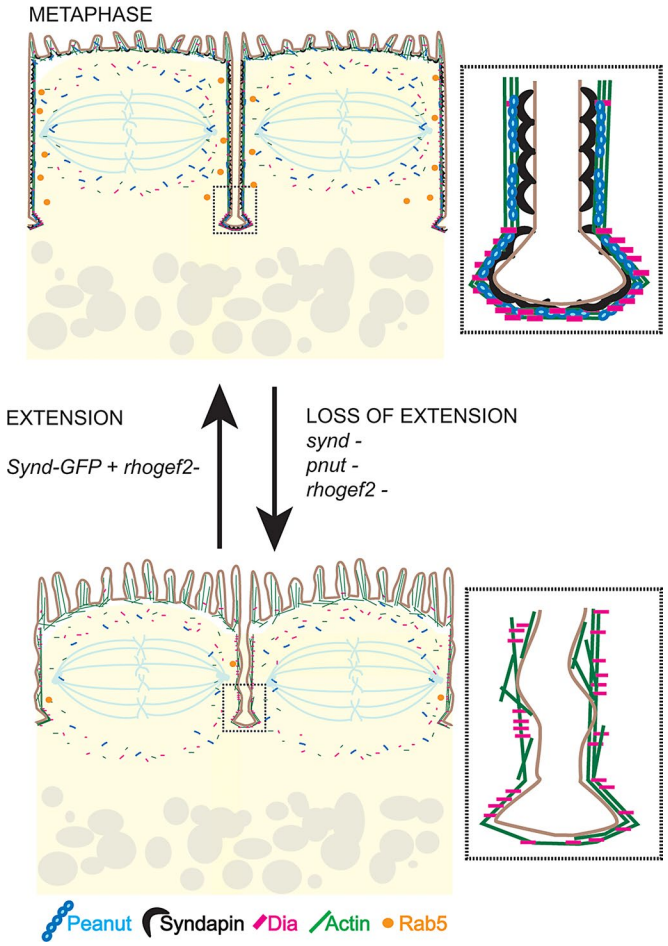


FIGURE 8: Schematic showing that the furrow defect in *synd*, *rhogef2*, and *pnut* mutants is reversed by Synd overexpression in *rhogef2*$^{RNAi}$. Pseudocleavage furrow extension in metaphase of the syncytial cycle in *synd*, *pnut*, and *rhogef2* mutants is decreased due to recruitment defects in Synd, Pnut, Dia, and actin, and reversed in *rhogef2* mutants by overexpression of Synd.

activity by increasing RhoA levels (Korobova and Svitkina, 2008). Such a mechanism can explain increased Dia function when Synd is overexpressed in RhoGEF2 knockdown embryos, which, along with recruitment of Pnut to the membrane, can help organize actin and elongate cleavage furrows (Figure 8).

Actin stabilization into continuous structures reversed the furrow length defect in *synd* mutant embryos. Jasp blocks actin turnover at the contractile ring (Murthy and Wadsworth, 2008) and affects cleavage furrow invagination while preserving furrow integrity (Cao *et al.*, 2008), and hence showed fewer punctae in *synd* and *rhogef2* mutant embryos. CytoD, on the other hand, allows actin polymerization (Goddette and Frieden, 1986; Franki *et al.*, 1992), and as a result, *synd* and *rhogef2* mutant embryos treated with CytoD displayed more organized actin structures and elongated furrows (Figure 7E). This provides mechanistic insight into how Synd functions in regulating actin polymerization and may be further investigated through kinetic studies of actin polymerization.

Overexpression of Synd and not Pnut in the *rhogef2*$^{RNAi}$-containing embryos partially reversed pseudocleavage furrow recruitment and morphology defects seen in *rhogef2*$^{RNAi}$ and increased the furrow length compared with wild type. Synd activity is thus needed at the pseudocleavage furrow for extension, and some as yet uncharacterized proteins play a role in furrow limitation. It is interesting to compare the functions of F-BAR domain proteins, Synd with Cip4 in furrow elongation and Dia recruitment. Cip4 antagonizes Dia function, and its overexpression has *dia* loss-of-function phenotypes like missing furrows (Yan *et al.*, 2013). It is possible that opposing activities of F-BAR proteins Synd and Cip4 with respect to Dia are in a balance, and future experiments can test whether this function plays a role in limiting the growth of pseudocleavage furrows.

Because Synd's SH3 domain interacts with Dynamin (Kumar *et al.*, 2009a), and Dynamin has a role in endocytosis and furrow extension in syncytial divisions and cellularization (Sokac and Wieschaus, 2008a; Rikhy *et al.*, 2015), it remained to be investigated whether Clathrin-dependent endocytosis defects in *synd* mutants also affect furrow elongation. We showed that *synd* mutant embryos have defects in cleavage furrow–tubule length and Rab5 vesicle numbers (Figure 6 and Supplemental Figure S4). Decrease in Rab5 vesicle numbers is also seen in *rhogef2* mutant embryos. However, Synd-GFP overexpression in *rhogef2* mutant embryos is able to reverse the furrow-extension defect without rescuing the Rab5 endocytic vesicle defect. Taken together, our data show that Synd has a role in endocytosis, but the reversal of furrow phenotypes in *rhogef2* mutant embryos is due to the ability of Synd to recruit and organize actin and proteins of the actin-remodeling machinery such as Dia and Pnut.

Our analysis of membrane architecture and pseudocleavage furrow length in *rhogef2*, *pnut*, and *synd* mutants found that shorter furrows in each of these mutants were also loose/unstable and had slow lateral movement during the nuclear cycle (Figures 2 and 5 and Supplemental Figure S3). Septins brace the plasma membrane against aberrant cell-shape deformation and are able to tubulate phosphatidylinositol-4,5-bisphosphate liposome membranes when treated with a brain extract (Tanaka-Takiguchi *et al.*, 2015). It is probable that Septin-mediated membrane tubulation activity and cell-shape effects are dependent on the presence of F-BAR proteins like Synd. Sept7 mutants in *Xenopus* show unstable and undulating membranes during gastrulation (Kim *et al.*, 2010). This substantiates Synd's role in maintenance of membrane integrity and shape by affecting actin organization and Pnut recruitment.

Overall mutant and epistatic analyses presented here find a significant role for the F-BAR domain protein Synd in mediating pseudocleavage furrow extension. Our study favors a model in which Synd, along with Anillin and RhoGEF2, provide a platform for

(green) in wild-type embryos stained with phalloidin is composed of few cytosolic punctae and organized linear structures. In *synd* mutants, there are mostly large punctae and disorganized structures along the furrow. In *rhogef2*$^{RNAi}$, actin is disorganized and linear structures are missing. *rhogef2*$^{RNAi}$ with Synd-GFP rescues this phenotype and yields more linear structures and small cytosolic punctae (D). (E) Treatment with Jasp increased short actin structures and reduced punctae but showed disorganized furrows in *synd*$^{1d}$/Df (100%; $n = 11$) and *rhogef2*$^{RNAi}$ (100%; $n = 11$). CytoD treatment in *synd*$^{1d}$/Df (60%; $n = 12$) and *rhogef2*$^{RNAi}$ (50%; $n = 10$) embryos restores furrow morphology by converting disrupted actin into organized structures; in wild type, it reorganizes actin into thick, short rods compared with DMSO control (100%; $n = 10$). Yellow arrow indicates apical accumulation of actin (C). Scale bars: 10 μm.

recruitment of Dia and Pnut to allow persistent and stable growth of actin to promote furrow elongation (Figure 8). Further experiments combining protein interactions and deduction of the biophysical nature of Synd-Pnut-actin association with the plasma membrane will elucidate the molecular mechanism that makes Synd an important component of pseudocleavage furrow-extension or contractile-ring assembly at large.

## MATERIALS AND METHODS

### *Drosophila* strains and genetics

Flies were raised on standard cornmeal agar at 25°C. Embryos from Canton S flies were used in control experiments. Homozygous escaper adults from the transposon-tagged mutant *synd*$^{1d}$/TM6B, Tb$^{1}$ (V. Kumar, IISER, Bhopal, India [Kumar *et al.*, 2009a]) or adults in with *trans*-allelic combination of *synd*$^{1d}$/*Df(3R)BSC43* [BL-7413] were used to generate *synd* mutant embryos. These embryos showed a loss of Synd immunostaining and high percentage of embryonic lethality by hatch assay (Figure 1). The *synd* mutant phenotype was rescued using Synd-GFP (T. Takeda and D. Glover, University of Cambridge, UK [Takeda *et al.*, 2013]). *synd*$^{RNAi}$ (BDSC stock) was crossed to nanos-Gal4 and embryos laid by females of the genotype *synd*$^{RNAi}$/nanos-Gal4 showed a lower embryonic lethality than the mutant (Figure 1).

For immunohistochemistry, the following mutant stocks were used: w*; *dia*$^{5}$ FRT40A/CyO [BL-9138], y$^{1}$ w*; *rhogef2*$^{4.1}$ FRTG13/CyO [BL-9122], and *pnut*$^{XP}$ FRT$^{G13}$/SM6a-TM6B, Tb$^{1}$ (M. Mavrakis, Fresnel Institute, Paris). Females carrying the mutant and heat-shock FLP were crossed to respective FRT *ovo*$^{D}$ males -*ovo*$^{D}$ FRT40A/CyO [BL-2121] or *ovo*$^{D}$ FRTG13/CyO to generate germline clones by heat-shocking third instar larvae, pupae, and adult flies for 1 h each at 37.5°C. The transheterozygous animals *scra*$^{k08255}$/scra$^{8}$[BL-4403, 4286] gave *anillin* (*scraps*) mutant embryos. *shi*$^{ts2}$ (R.R.) mutants were transferred to a restrictive temperature (32°C) for 5 min before fixation.

Gap43-Venus (Mavrakis *et al.*, 2009) with H2A-RFP [BL-25377] was used to show pseudocleavage furrow morphology changes across nuclear cycle 13. Metaphase furrow lengths in nuclear cycles 12 and 13 were measured by a tGPH; nanos-Gal4 recombinant line [BL-8163, 4937]. RNAi lines for *rhogef2* [BL-34643], *dia* [BL-33424], and *pnut* (VDRC, Austria) were used. Ub-Synd-GFP/+; *synd*$^{1d}$/Df was used to measure furrow and protein dynamics and Ub-Synd-GFP was combined with *rhogef2*$^{RNAi}$ to test rescue. UASp-mCherry::Pnut (T. Lecuit, IBDM, France [Guillot and Lecuit, 2013]) was used to overexpress Pnut in the background of *rhogef2*$^{RNAi}$.

### Immunohistochemistry

Embryos were collected for 3 h at 25°C (and at 28°C for RNAi experiments) on 3% sucrose agar plates; washed and dechorionated in 100% bleach for 1 min; fixed in 1:1::4% paraformaldehyde in phosphate-buffered saline (PBS):heptane for 15 min; hand/methanol devitellinized; permeabilized with 0.3% Triton-X in PBS (PBST); blocked in 2% bovine serum albumin (Sigma-Aldrich) in PBST; and immunostained with primary antibodies: Synd (rat, 1:150 [V. Kumar]), Dia (rabbit, 1:1000 [S. Wasserman, University of California, San Diego]), Pnut (mouse, 1:5 [DSHB-4C9H4]), Anillin (rabbit, 1:1000 [C. Field, Harvard, and Julie Brill, The Hospital for Sick Children, Toronto, Canada]), Rab5 (rabbit, 1:200 [Abcam]). RhoGEF2 antibody (rabbit, 1:500 [J. Grosshans]) staining was done after heat-fixation followed by 1:1::heptane:methanol devitellinization. Fluorescently coupled secondary antibodies (Alexa Fluor 488, 568, and 633; 1:1000; Life Technologies, Bangalore, India) were used. DNA was labeled with Hoechst 3342 (10 mg/ml; 1:1000; Life Technologies) and F-actin was labeled with Alexa Fluor 488/568 phalloidin (1:100; Life Technologies). The embryos were mounted in SlowFade Gold (Life Technologies). These samples were imaged using a Plan-Apochromat 40×/1.3 NA oil-immersion objective on a confocal laser scanning microscope (LSM 710; Zeiss, Bangalore, India). *z*-Stacks were acquired on sequentially scanned images with a spacing of 1.08 µm between slices. *n* values indicate number of syncytial cycle 12 or 13 embryos screened. Embryos defective for a phenotype were calculated as a percentage of *n*. For quantitative analysis of Rab5-positive vesicles and Amph furrow tubules, images were acquired using a Plan-Apochromat 63×/1.3 NA oil-immersion objective on a confocal laser scanning microscope (LSM 710, Zeiss) with pinhole set at 1 AU for best signal/noise.

Zeiss LSM 800 with Airyscan (0.15 µm slice thickness) was used to acquire and process high-resolution images of Hoechst and phalloidin-stained embryos.

### Drug treatment with actin-binding drugs

Dechorionated embryos were added to a solution of 1:1::(R)-(+)-Limonene (Sigma):heptane to which the drug dissolved in DMSO was added to achieve the desired final concentration (200 nM Jasp, 50 µM/ 100 µM CytoD, 10 µM LatA, or DMSO without drug in case of control) and incubated with shaking for 5 min (adapted from Rand *et al.*, 2010; Schulman *et al.*, 2013). The solution was then replaced with fresh heptane and subsequently fixed, hand devitenillized, and immunostained as described in the protocol described above.

### Live-embryo time-lapse imaging

Embryos were collected for 1 h, dechorionated, and mounted in a LabTek chamber with PBS (Mavrakis *et al.*, 2008) and imaged in four dimensions (every 30 s with 0.48/1.08 µm thickness) using a Zeiss Plan-Apochromat 40×/1.4 NA oil-immersion objective on a Zeiss LSM 780 inverted confocal microscope. Staging of embryos during the cell cycle was done by corroborating the presence of the nuclear envelope and its breakdown with metaphase furrow length. Because some tGPH is in the cytoplasm, these events are easy to distinguish in the live movies to accurately stage the embryos.

### Image processing

Images were processed with ImageJ (National Institutes of Health) and compiled with Adobe Photoshop CS5. Immunostains are shown from single optical planes for sagittal (*x*,*z*) or surface views (*x*,*y*). A Gaussian smoothing filter with a radius of one pixel was used to reduce noise. Processed Images of F-actin and DNA obtained from Airyscan were imported into Imaris8.1 software (Bitplane, Hyderabad, India), and snapshots of single *z*-slices (Slice), 3D surface rendering (Surface), and MIP were represented.

### FRAP

For FRAP (Mavrakis *et al.*, 2008), three prebleach scans and 30 bleach iterations (0.03 s each) were taken on living Synd-GFP and tGPH embryos in ~2.5 µm$^2$ regions on the apical and FT membrane. Recovery of fluorescence intensity was recorded until a steady state was reached. The data were background corrected and normalized to the prebleach intensity and transformed on a 0–1 scale. The individual postbleach intensities were fit with a one-phase exponential association equation ($Y = Y_{max}(1 - e^{-K.X}) + c$) using GraphPad. Nonlinear regression was used obtain the $Y_{max}$ or mobile fraction for Synd-GFP ($R^2 = 0.83 \pm 0.1$ SD and $0.83 \pm 0.03$ SD for apical and FT membranes, respectively). The immobile fraction (1-mobile fraction)

was calculated and plotted as scatter plots using GraphPad for apical and FT membranes.

### Image analysis and quantification

Intensity density on membrane regions from confocal images of Synd and Amph was computed using ImageJ. After background subtraction, the ratio of Synd:Amph was plotted as a box plot using GraphPad. A nonparametric Mann-Whitney *U*-test was performed to test for significance between means. Intensity of Synd-GFP (in apical, lateral, and FT membrane regions) was similarly measured from images in metaphase of cycles 11, 12, and 13 and plotted as a scatter plot using GraphPad. The mean intensity values were compared for significance using one-way analysis of variance (ANOVA), Tukey's multiple-comparison test. For furrow length, freehand lines along the lateral membrane to FT from orthogonal views at desired time points of time-lapse movies were measured, and the mean ± SEM of the furrow length was plotted using GraphPad. Lateral furrow broadness was represented as intensity peaks on a line across furrows in orthogonal views using the Plot profile analysis tool of ImageJ. For numbers of Rab5-positive vesicles, the ImageJ plug-in 3D-Objects Counter was used. Only objects in the volume of the pseudocell and below 250 nm diameter were counted. The absolute number was normalized to the number of pseudocells in the region of interest (ROI) and plotted for 3 embryos/genotype using GraphPad. For quantification of furrow-tubule length, images of fixed Amph-stained embryos in prometaphase during cycle 13 were used; freehand lines were drawn along the tubules, and their length was measured using ImageJ and their number was counted. The length and number (per furrow) were plotted for a minimum of five embryos/genotype using GraphPad.

### Kymograph analysis

Lateral membrane movement of metaphase furrows in the *x,y* plane was plotted using the Multiple Kymograph plug-in of ImageJ on single-plane time-series movies of tGPH::GFP-labeled embryos. Lines were drawn to generate tracks across four metaphase 13 furrows. The displacement was quantified by selecting the initial to final points of furrow movement using the line tool and, subsequently, the macro "read velocities from tsp" to obtain displacement/velocities. The displacement was plotted using GraphPad. An unpaired *t* test (two-tailed) with Welch's correction was used to test significance between means, and an *F*-test was used to compare significant difference in variances.

## ACKNOWLEDGMENTS

This study was motivated by K. S. Krishnan, and we dedicate this study to him. We thank Manos Mavrakis, Vimlesh Kumar, Thomas Pucadyil, Aurnab Ghose, Girish Ratnaparkhi, L. S. Shashidhara, Anuradha Ratnaparkhi, Girish Deshpande, and R.R. lab members for critical comments throughout this work. A.S. thanks Shamik Banerjee for discussions and critical reading of the manuscript. Ramya Balaji, Prachi Richa, and Vishnu Saraswathy helped with preliminary characterization of *synd* mutants. We thank Vimlesh Kumar, Steve Wasserman, Hugo Bellen, Tetsuya Takeda, Manos Mavrakis, Thomas Lecuit, Christine Field, and Julie Brill for reagents. We thank the Bloomington Stock Center for fly stocks. We thank the IISER, Pune, *Drosophila* facility and imaging facility for help with fly maintenance and microscopy. The LSM 800 Airyscan microscope for high-resolution imaging was kindly shared by Zeiss, India. A.S. thanks the Council of Scientific and Industrial Research for a graduate fellowship. R.R. thanks the Department of Biotechnology and IISER, Pune, for funding this work.

## REFERENCES

Afshar K, Stuart B, Wasserman SA (2000). Functional analysis of the *Drosophila* diaphanous FH protein in early embryonic development. Development 127, 1887–1897.

Ahuja R, Pinyol R, Reichenbach N, Custer L, Klingensmith J, Kessels MM, Qualmann B (2007). Cordon-Bleu is an actin nucleation factor and controls neuronal morphology. Cell 131, 337–350.

Alsop GB, Zhang D (2003). Microtubules are the only structural constituent of the spindle apparatus required for induction of cell cleavage. J Cell Biol 162, 383–390.

Ang SF, Zhao ZS, Lim L, Manser E (2010). DAAM1 is a formin required for centrosome re-orientation during cell migration. PLoS One 5, e13064.

Barmchi MP, Rogers S, Häcker U (2005). DRhoGEF2 regulates actin organization and contractility in the *Drosophila* blastoderm embryo. J Cell Biol 168, 575–585.

Bezanilla M, Gladfelter AS, Kovar DR, Lee W-L (2015). Cytoskeletal dynamics: a view from the membrane. J Cell Biol 209, 329–337.

Bringmann H, Hyman AA (2005). A cytokinesis furrow is positioned by two consecutive signals. Nature 436, 731–734.

Britton JS, Lockwood WK, Li L, Cohen SM, Edgar BA (2002). *Drosophila*'s insulin/PI3-kinase pathway coordinates cellular metabolism with nutritional conditions. Dev Cell 2, 239–249.

Bubb MR, Senderowicz AMJ, Sausville EA, Duncan KLK, Korn ED (1994). Jasplakinolide, a cytotoxic natural product, induces actin polymerization and competitively inhibits the binding of phalloidin to F-actin. J Biol Chem 269, 14869–14871.

Bubb MR, Spector I, Beyer BB, Fosen KM (2000). Effects of jasplakinolide on the kinetics of actin polymerization. An explanation for certain in vivo observations. J Biol Chem 275, 5163–5170.

Buchsbaum RJ (2007). Rho activation at a glance. J Cell Sci 120, 1149–1152.

Cabernard C (2012). Cytokinesis in *Drosophila melanogaster*. Cytoskeleton 69, 791–809.

Cao J, Albertson R, Riggs B, Field CM, Sullivan W (2008). Nuf, a Rab11 effector, maintains cytokinetic furrow integrity by promoting local actin polymerization. J Cell Biol 182, 301–313.

Carlier MF, Criquet P, Pantaloni D, Korn ED (1986). Interaction of cytochalasin D with actin filaments in the presence of ADP and ATP. J Biol Chem 261, 2041–2050.

Castrillon DH, Wasserman SA (1994). Diaphanous is required for cytokinesis in *Drosophila* and shares domains of similarity with the products of the limb deformity gene. Development 120, 3367–3377.

Collings D, Wasteneys G, Williamson R (1995). Cytochalasin rearranges cortical actin of the alga *Nitella* into short, stable rods. Plant Cell Physiol 36, 765–772.

Coué M., Brenner SL, Spector I, Korn ED (1987). Inhibition of actin polymerization by latrunculin A. FEBS Lett 213, 316–318.

Crest J, Concha-Moore K, Sullivan W (2012). RhoGEF and positioning of Rappaport-like furrows in the early *Drosophila* embryo. Curr Biol 22, 2037–2041.

Daniels BR, Rikhy R, Renz M, Dobrowsky TM, Lippincott-Schwartz J (2012). Multiscale diffusion in the mitotic *Drosophila* melanogaster syncytial blastoderm. Proc Natl Acad Sci USA 109, 8588–8593.

D'Avino PP (2009). How to scaffold the contractile ring for a safe cytokinesis—lessons from Anillin-related proteins. J Cell Sci 122, 1071–1079.

D'Avino PP, Takeda T, Capalbo L, Zhang W, Lilley KS, Laue ED, Glover DM (2008). Interaction between Anillin and RacGAP50C connects the actomyosin contractile ring with spindle microtubules at the cell division site. J Cell Sci 121, 1151–1158.

de Kreuk B-J, Nethe M, Fernandez-Borja M, Anthony EC, Hensbergen PJ, Deelder AM, Plomann M, Hordijk PL (2011). The F-BAR domain protein PACSIN2 associates with Rac1 and regulates cell spreading and migration. J Cell Sci 124, 2375–2388.

Dharmalingam E, Haeckel A, Pinyol R, Schwintzer L, Koch D, Kessels MM, Qualmann B (2009). F-BAR proteins of the syndapin family shape the plasma membrane and are crucial for neuromorphogenesis. J Neurosci 29, 13315–13327.

Edeling MA, Sanker S, Shima T, Umasankar PK, Höning S, Kim HY, Davidson LA, Watkins SC, Tsang M, Owen DJ, Traub LM (2009). Structural requirements for PACSIN/syndapin operation during zebrafish embryonic notochord development. PLoS One 4, e8150.

Fares H, Peifer M, Pringle JR (1995). Localization and possible functions of *Drosophila* septins. Mol Biol Cell 6, 1843–1859.

Fededa JP, Gerlich DW (2012). Molecular control of animal cell cytokinesis. Nat Cell Biol 14, 440–447.

Field CM, Alberts BM (1995). Anillin, a contractile ring protein that cycles from the nucleus to the cell cortex. J Cell Biol 131, 165–178.
Field CM, Coughlin M, Doberstein S, Marty T, Sullivan W (2005). Characterization of anillin mutants reveals essential roles in septin localization and plasma membrane integrity. Development 132, 2849–2860.
Figard L, Xu H, Garcia HG, Golding I, Sokac AM (2013). The plasma membrane flattens out to fuel cell-surface growth during *Drosophila* cellularization. Dev Cell 27, 648–655.
Foe VE, Alberts BM (1983). Studies of nuclear and cytoplasmic behaviour during the five mitotic cycles that precede gastrulation in *Drosophila* embryogenesis. J Cell Sci 61, 31–70.
Foe VE, Field CM, Odell GM (2000). Microtubules and mitotic cycle phase modulate spatiotemporal distributions of F-actin and myosin II in *Drosophila* syncytial blastoderm embryos. Development 127, 1767–1787.
Foissner I, Wasteneys OG (1999). Microtubules at wound sites of *Nitella* internodal cells passively co-align with actin bundles when exposed to hydrodynamic forces generated by cytoplasmic streaming. Planta 208, 480–490.
Foissner I, Wasteneys GO (2000). Microtubule disassembly enhances reversible cytochalasin-dependent disruption of actin bundles in characean internodes. Protoplasma 214, 33–44.
Franki N, Ding G, Gao Y, Hays RM (1992). Effect of cytochalasin D on the actin cytoskeleton of the toad bladder epithelial cell. Am J Physiol Cell Physiol 263, C995–C1000.
Frescas D, Mavrakis M, Lorenz H, Delotto R, Lippincott-Schwartz J (2006). The secretory membrane system in the *Drosophila* syncytial blastoderm embryo exists as functionally compartmentalized units around individual nuclei. J Cell Biol 173, 219–230.
Frost A, Perera R, Roux A, Spasov K, Destaing O, Egelman EH, De Camilli P, Unger VM (2008). Structural basis of membrane invagination by F-BAR domains. Cell 132, 807–817.
Goddette DW, Frieden C (1986). Actin polymerization. The mechanism of action of cytochalasin D. J Biol Chem 261, 15974–15980.
Graziano BR, Yu H-YE, Alioto SL, Eskin Ja, Ydenberg Ca, Waterman DP, Garabedian M, Goode BL (2014). The F-BAR protein Hof1 tunes formin activity to sculpt actin cables during polarized growth. Mol Biol Cell 25, 1730–1743.
Gregory SL, Ebrahimi S, Milverton J, Jones WM, Bejsovec A, Saint R (2008). Cell division requires a direct link between microtubule-bound RacGAP and Anillin in the contractile ring. Curr Biol 18, 25–29.
Grevengoed EE, Fox DT, Gates J, Peifer M (2003). Balancing different types of actin polymerization at distinct sites: roles for Abelson kinase and Enabled. J Cell Biol 163, 1267–1279.
Grosshans J, Wenzl C, Herz H-M, Bartoszewski S, Schnorrer F, Vogt N, Schwarz H, Müller H-A (2005). RhoGEF2 and the formin Dia control the formation of the furrow canal by directed actin assembly during *Drosophila* cellularisation. Development 132, 1009–1020.
Guillot C, Lecuit T (2013). Mechanics of epithelial tissue homeostasis and morphogenesis. Science 340, 1185–1189.
Haglund K, Nezis IP, Stenmark H (2011). Structure and functions of stable intercellular bridges formed by incomplete cytokinesis during development. Commun Integr Biol 4, 1–9.
Heng Y-W, Koh C-G (2010). Actin cytoskeleton dynamics and the cell division cycle. Int J Biochem Cell Biol 42, 1622–1633.
Holly RM, Mavor LM, Zuo Z, Blankenship JT (2015). A rapid, membrane-dependent pathway directs furrow formation through RalA in the early *Drosophila* embryo. Development 142, 2316–2328.
Jaiswal R, Stepanik V, Rankova A, Molinar O, Goode BL, McCartney BM (2013). *Drosophila* homologues of Adenomatous Polyposis Coli (APC) and the formin Diaphanous collaborate by a conserved mechanism to stimulate actin filament assembly. J Biol Chem 288, 13897–13905.
Kellogg DR, Mitchison TJ, Alberts BM (1988). Behaviour of microtubules and actin filaments in living *Drosophila* embryos. Development 103, 675–686.
Kim SK *et al*. (2010). Planar cell polarity acts through septins to control collective cell movement and ciliogenesis. Science 329, 1337–1340.
Kinoshita M, Field CM, Coughlin ML, Straight AF, Mitchison TJ (2015). Self- and actin-templated assembly of mammalian septins. Dev Cell 3, 791–802.
Korobova F, Svitkina T (2008). Arp2/3 complex is important for filopodia formation, growth cone motility, and neuritogenesis in neuronal cells. Mol Biol Cell 19, 1561–1574.
Kostan J *et al*. (2014). Direct interaction of actin filaments with F-BAR protein pacsin2. EMBO Rep 15, 1154–1162.
Kumar V, Alla SR, Krishnan KS, Ramaswami M (2009a). Syndapin is dispensable for synaptic vesicle endocytosis at the *Drosophila* larval neuromuscular junction. Mol Cell Neurosci 40, 234–241.
Kumar V, Fricke R, Bhar D, Reddy-Alla S, Krishnan KS, Bogdan S, Ramaswami M (2009b). Syndapin promotes formation of a postsynaptic membrane system in *Drosophila*. Mol Biol Cell 20, 2254–2264.
Laporte D, Coffman VC, Lee I-J, Wu J-Q (2011). Assembly and architecture of precursor nodes during fission yeast cytokinesis. J Cell Biol 192, 1005–1021.
Lecuit T (2004). Junctions and vesicular trafficking during *Drosophila* cellularization. J Cell Sci 117, 3427–3433.
Lecuit T, Wieschaus E (2000). Polarized insertion of new membrane from a cytoplasmic reservoir during cleavage of the *Drosophila* embryo. J Cell Biol 150, 849–860.
Liu J, Fairn GD, Ceccarelli DF, Sicheri F, Wilde A (2012). Cleavage furrow organization requires PIP(2)-mediated recruitment of anillin. Curr Biol 22, 64–69.
Liu S, Xiong X, Zhao X, Yang X, Wang H (2015). F-BAR family proteins, emerging regulators for cell membrane dynamic changes-from structure to human diseases. J Hematol Oncol 8, 47.
Maddox AS, Lewellyn L, Desai A, Oegema K (2007). Anillin and the septins promote asymmetric ingression of the cytokinetic furrow. Dev Cell 12, 827–835.
Mavrakis M, Azou-Gros Y, Tsai F-C, Alvarado J, Bertin A, Iv F, Kress A, Brasselet S, Koenderink GH, Lecuit T (2014). Septins promote F-actin ring formation by crosslinking actin filaments into curved bundles. Nat Cell Biol 16, 322–334.
Mavrakis M, Rikhy R, Lilly M, Lippincott-Schwartz J (2008). Fluorescence imaging techniques for studying *Drosophila* embryo development. Curr Protoc Cell Biol chapter 4, unit 4.18.
Mavrakis M, Rikhy R, Lippincott-Schwartz J (2009). Plasma membrane polarity and compartmentalization are established before cellularization in the fly embryo. Dev Cell 16, 93–104.
Meitinger F, Richter H, Heisel S, Hub B, Seufert W, Pereira G (2013). A safeguard mechanism regulates Rho GTPases to coordinate cytokinesis with the establishment of cell polarity. PLoS Biol 11, e1001495.
Murthy K, Wadsworth P (2008). Dual role for microtubules in regulating cortical contractility during cytokinesis. J Cell Sci 121, 2350–2359.
Oegema K, Savoian MS, Mitchison TJ, Field CM (2000). Functional analysis of a human homologue of the *Drosophila* actin binding protein Anillin suggests a role in cytokinesis. J Cell Biol 150, 539–552.
Oh Y, Schreiter J, Nishihama R, Wloka C, Bi E (2013). Targeting and functional mechanisms of the cytokinesis-related F-BAR protein Hof1 during the cell cycle. Mol Biol Cell 24, 1305–1320.
Ou GS, Chen ZL, Yuan M (2002). Jasplakinolide reversibly disrupts actin filaments in suspension-cultured tobacco BY-2 cells. Protoplasma 219, 168–175.
Pelissier A, Chauvin J-P, Lecuit T (2003). Trafficking through Rab11 endosomes is required for cellularization during *Drosophila* embryogenesis. Curr Biol CB 13, 1848–1857.
Piekny AJ, Maddox AS (2010). The myriad roles of Anillin during cytokinesis. Semin Cell Dev Biol 21, 881–891.
Qualmann B, Kelly RB (2000). Syndapin isoforms participate in receptor-mediated endocytosis and actin organization. J Cell Biol 148, 1047–1062.
Qualmann B, Roos J, DiGregorio PJ, Kelly RB (1999). Syndapin I, a synaptic dynamin-binding protein that associates with the neural Wiskott-Aldrich syndrome protein. Mol Biol Cell 10, 501–513.
Ramachandran P, Barria R, Ashley J, Budnik V (2009). A critical step for postsynaptic F-actin organization: regulation of Baz/Par-3 localization by aPKC and PTEN. Dev Neurobiol 69, 583–602.
Ramesh P, Baroji YF, Reihani SNS, Stamou D, Oddershede LB, Bendix PM (2013). FBAR syndapin 1 recognizes and stabilizes highly curved tubular membranes in a concentration dependent manner. Sci Rep 3, 1565.
Rand MD, Kearney AL, Dao J, Clason T (2010). Permeabilization of Drosophila embryos for introduction of small molecules. Insect Biochem Mol Biol 40, 792–804.
Rao Y, Ma Q, Vahedi-Faridi A, Sundborger A, Pechstein A, Puchkov D, Luo L, Shupliakov O, Saenger W, Haucke V (2010). Molecular basis for SH3 domain regulation of F-BAR–mediated membrane deformation. Proc Natl Acad Sci USA 107, 8213–8218.
Renshaw MJ, Liu J, Lavoie BD, Wilde A (2014). Anillin-dependent organization of septin filaments promotes intercellular bridge elongation and Chmp4B targeting to the abscission site. Open Biol 4, 130190.

Rikhy R, Mavrakis M, Lippincott-Schwartz J (2015). Dynamin regulates metaphase furrow formation and plasma membrane compartmentalization in the syncytial *Drosophila* embryo. Biol Open 4, 301–311.
Roberts-Galbraith RH, Gould KL (2010). Setting the F-BAR: functions and regulation of the F-BAR protein family. Cell Cycle 9, 4091–4097.
Roos J, Kelly RB (1998). Dap160, a neural-specific eps15 homology and multiple SH3 domain-containing protein that interacts with *Drosophila* dynamin. J Biol Chem 273, 19108–19119.
Royou A, Field C, Sisson JC, Sullivan W, Karess R (2004). Reassessing the role and dynamics of nonmuscle myosin II during furrow formation in early *Drosophila* embryos. Mol Biol Cell 15, 838–850.
Saha S, Pollard TD (2012). Anillin-related protein Mid1p coordinates the assembly of the cytokinetic contractile ring in fission yeast. Mol Biol Cell 23, 3982–3992.
Schmidt K, Nichols BJ (2004). A barrier to lateral diffusion in the cleavage furrow of dividing mammalian cells. Curr Biol 14, 1002–1006.
Schulman VK, Folker ES, Baylies MK (2013). A method for reversible drug delivery to internal tissues of Drosophila embryos. Fly (Austin) 7, 193–203.
Schwintzer L, Koch N, Ahuja R, Grimm J, Kessels MM, Qualmann B (2011). The functions of the actin nucleator Cobl in cellular morphogenesis critically depend on syndapin I. EMBO J 30, 3147–3159.
Silverman-Gavrila RV, Hales KG, Wilde A (2008). Anillin-mediated targeting of Peanut to pseudocleavage furrows is regulated by the GTPase Ran. Mol Biol Cell 19, 3735–3744.
Simpson F, Hussain NK, Qualmann B, Kelly RB, Kay BK, McPherson PS, Schmid SL (1999). SH3-domain-containing proteins function at distinct steps in clathrin-coated vesicle formation. Nat Cell Biol 1, 119–124.
Sokac AM, Wieschaus E (2008a). Local actin-dependent endocytosis is zygotically controlled to initiate *Drosophila* cellularization. Dev Cell 14, 775–786.
Sokac AM, Wieschaus E (2008b). Zygotically controlled F-actin establishes cortical compartments to stabilize furrows during *Drosophila* cellularization. J Cell Sci 121, 1815–1824.
Stevenson V, Hudson A, Cooley L, Theurkauf WE (2002). Arp2/3-dependent pseudocleavage [correction of psuedocleavage] furrow assembly in syncytial *Drosophila* embryos. Curr Biol 12, 705–711.
Straight AF, Field CM, Mitchison TJ (2005). Anillin binds nonmuscle myosin II and regulates the contractile ring. Mol Biol Cell 16, 193–201.
Su J, Chow B, Boulianne GL, Wilde A (2013). The BAR domain of amphiphysin is required for cleavage furrow tip–tubule formation during cellularization in *Drosophila* embryos. Mol Biol Cell 24, 1444–1453.
Takeda T, Robinson IM, Savoian MM, Griffiths JR, Whetton AD, McMahon HT, Glover DM (2013). *Drosophila* F-BAR protein Syndapin contributes to coupling the plasma membrane and contractile ring in cytokinesis. Open Biol 3, 130081.
Tanaka-Takiguchi Y, Kinoshita M, Takiguchi K (2015). Septin-mediated uniform bracing of phospholipid membranes. Curr Biol 19, 140–145.
Watanabe S *et al*. (2013). Loss of a Rho-regulated actin nucleator, mDia2, Impairs cytokinesis during mouse fetal erythropoiesis. Cell Rep 5, 926–932.
Watanabe S, Ando Y, Yasuda S, Hosoya H, Watanabe N, Ishizaki T, Narumiya S (2008). mDia2 induces the actin scaffold for the contractile ring and stabilizes its position during cytokinesis in NIH 3T3 cells. Mol Biol Cell 19, 2328–2338.
Watanabe S, Okawa K, Miki T, Sakamoto S, Morinaga T, Segawa K, Arakawa T, Kinoshita M, Ishizaki T, Narumiya S (2010). Rho and anillin-dependent control of mDia2 localization and function in cytokinesis. Mol Biol Cell 21, 3193–3204.
Webb RL, Zhou MN, McCartney BM (2009). A novel role for an APC2-Diaphanous complex in regulating actin organization in *Drosophila*. Development 136, 1283–1293.
Willet AH, McDonald NA, Bohnert KA, Baird MA, Allen JR, Davidson MW, Gould KL (2015). The F-BAR Cdc15 promotes contractile ring formation through the direct recruitment of the formin Cdc12. J Cell Biol 208, 391–399.
Yan S, Lv Z, Winterhoff M, Wenzl C, Zobel T, Faix J, Bogdan S, Grosshans J (2013). The F-BAR protein Cip4/Toca-1 antagonizes the formin Diaphanous in membrane stabilization and compartmentalization. J Cell Sci 126, 1796–1805.
Yonetani A, Lustig RJ, Moseley JB, Takeda T, Goode BL, Chang F (2008). Regulation and targeting of the fission yeast formin cdc12p in cytokinesis. Mol Biol Cell 19, 2208–2219.
Yoshida S, Bartolini S, Pellman D (2009). Mechanisms for concentrating Rho1 during cytokinesis. Genes Dev 23, 810–823.